Smart Structures and Systems, *Vol. 24, No. 2 (2019) 267-292*
DOI: https://doi.org/10.12989/sss.2019.24.2.267

Coupled evaluation of the free vibration characteristics of magneto-electro-elastic skew plates in hygrothermal environment

Vinyas Mahesh[1,2], Subhaschandra Kattimani[3], Dineshkumar Harursampath[1] and Nguyen-Thoi Trung[*4,5]

[1]*Department of Aerospace Engineering, Indian Institute of Science, Bangalore-560012, India*
[2]*Department of Mechanical Engineering, Nitte Meenakshi Institute of Technology Bangalore – 560064, Karnataka, India.*
[3]*Department of Mechanical Engineering, National Institute of Technology Karnataka, Surathkal-575025, India*
[4]*Division of Computational Mathematics and Engineering, Institute for Computational Science, Ton Duc Thang University, Ho Chi Minh City, Vietnam*
[5]*Faculty of Civil Engineering, Ton Duc Thang University, Ho Chi Minh City, Vietnam*

(Received April 9, 2018, Revised April 26, 2019, Accepted April 30, 2019)

Abstract. The present article addresses the coupled free vibration problem of skew magneto-electro-elastic plates (SMEE) considering the temperature-moisture dependent material properties. The plate kinematics follows Reddy's higher order shear deformation theory. With the aid of finite element methods, the governing equations of motion are derived considering the Hamilton's principle and solved by adopting condensation technique. The influence of different temperature and moisture dependent empirical constants on the frequency response of SMEE plate has been assessed. In addition, the natural frequencies corresponding to various fields are evaluated and the effect of empirical constants on these coupled frequencies is determined. A detailed parametric study has been carried out to assess the individual effects of temperature and moisture dependent empirical constants along with their combined effect, aspect ratio, length-to-width ratio, stacking sequence and boundary conditions. The results reveal that the external environment as well as the geometrical skewness has a significant influence on the stiffness of the SMEE plates.

Keywords: coupling; magneto-electro-elastic; hygrothermal; geometrical skewness; empirical constants

1. Introduction

The multiferroic materials such as Magneto-electro-elastic (MEE) are grasping the significant attention of the scientific communities due to their intensive energy conversion capabilities (Vinyas *et al.* 2018a, Vinyas and Kattimani 2018a). These materials display triple energy conversion among elastic, electric and magnetic fields. The MEE materials as a result of their beneficial coupling properties have become a potential candidate for various engineering applications which includes electronic devices, acoustic devices, magnetic field probes, medical ultrasonic imaging, sensors, and actuators, etc. The intelligent structures composed of MEE materials needs a thorough examination. In this regard, many pioneers have attempted to study the mechanical response of MEE structures. Pan and his fellow researchers (2001, 2002, 2005, 2016) inspected the free vibration behaviour of MEE plates via exact solutions. Using state vector approach, Wang and Pan (2011) and Chen *et al*. (2014) probed the vibration characteristics of laminated MEE plates. The examination of the natural frequencies of MEE plates with the aid of partial mixed layer-wise finite element methods was performed by Lage *et al.* (2004). Meanwhile, few more literature adopting different computational techniques such as approximate solution method (Ramirez *et al.* 2006a, Huang *et al.* 2007), semi-analytical FE procedure (Bhangale and Ganesan 2006), FE methods (Annigeri *et al.* 2007, Vinyas *et al.* 2017a, Daga *et al*. 2009), mesh lessmethod (Sladek et al. 2013a), discrete layer method (Ramirez *et al.* 2006b) and state space approach (Xin and Hu 2015, Chen *et al.* 2007) also have contributed in evaluating the free vibration characteristics of MEE plates. In addition to these literatures, several layer-wise theories are also proved to be handy in yielding accurate frequencies (Alaimo *et al.* 2013, Milazzo 2013, 2014a, b, Benedetti and Milazzo 2017). The nonlinear free vibration behaviour of MEE structures supported by an elastic foundation was studied by Razavi and Shooshtari (2015), as well as Shooshtari and Razavi (2015a).

The coupled responses of piezoelectric smart structures in the thermal environment have an interesting phenomenon associated with it (Saadatfar and Khafri 2015). On the same grounds, exploring the thermal effects on the behaviour of MEE structures has motivated the research community in the recent years. It is reported by many investigators that the thermal fields significantly affect the coupled characteristics of MEE structures. With the aid of FE procedure, Sunar (2002) researched the coupled phenomenon and derived the constitutive equations for the thermopiezomagnetic continuum. In another work, Badri and Kayiem (2013) investigated the static and dynamic analysis of magneto-electro-thermo-elastic (METE) plates. An exact solution was developed by Ootao and Tanigawa

*Corresponding author, Professor
E-mail: nguyenthoitrung@tdtu.edu.vn

ISSN: 1738-1584 (Print), 1738-1991 (Online)

(2005) to analyse the transient behavior of multilayered METE strip subjected to non-uniform and unsteady heating.

A unique behaviour of MEE structures can be experienced in the thermal environment due to additional pyro-coupling effects. Kondaiah *et al.* (2012, 2015, 2017) evaluated the influence of pyroelectric and pyromagnetic coupling on the structural behaviour of MEE beams, plates and cylinders. Further, the effect of temperature loads on the free vibration of MEE beams was studied by Kumaravel *et al.* (2007). More recently, Vinyas and Kattimani contributed to the research community through their works which discuss the effect of various forms of thermal loading on the coupled static response of stepped-functionally graded MEE beams (Vinyas and Kattimani 2017b, c, d, e, f) and plates (Vinyas and Kattimani 2017g). Extending their evaluation on the same grounds, the influence of moisture was also briefed out (Vinyas and Kattimani 2017h, Vinyas *et al.* 2018b). Akbarzadeh and Chen (2014) derived analytical solutions and compared the coupled response of functionally graded and homogeneous thermo-magneto-electro-elastic hollow cylinder.

Several articles have been reported on evaluating the coupled hygrothermo-magneto-electro-elastic response of MEE structures. Among them, investigation of the multiphysics MEE behaviour of rotating cylinders subjected to hygrothermal loads was analysed by Akbarzadeh and Chen (2012) considering the temperature and moisture dependent material properties. In their other work, they performed an analytical evaluation of the hygrothermal stresses in one-dimensional functionally graded piezoelectric media (2013). The effect of elastic foundation on the hygrothermo-magneto-electro-elastic behavior of FG-MEE hollow sphere was thoroughly examined by Saadatfar and Khafri (2014). Akbarzadeh and Pasini (2014) developed a closed form solution to evaluate the steady-state responses of functionally graded, multilayered infinitely long cylinders and thin circular disks under hygrothermal loading.

To assess the kinematics of the plate, many plate theories have been proposed. The classical plate theory (CPT) is considered to be elementary among those. It is worthy to mention that, CPT completely ignores the influence of shear deformation. As a result it cannot be adopted for thick plates (Ebrahimi and Shafiei 2017, Ebrahimi and Barati 2016). On the other hand, the first-order shear deformation theory (FSDT) overcomes this drawback but requires shear correction factor to get accurate results. Further, selection of the correct shear correction factor is quite critical and affects the results drastically. Therefore, many higher order shear deformation theories (HSDT) came into existence. The HSDT satisfies the zero shear stress conditions without the requirement of shear correction factors which facilitates a better representation of the structural kinematics. However, the literatures reported on exploiting the advantages of HSDT for MEE structural analysis is available in scarce. Moita *et al.* (2009) proposed an analytical solution to solve for the vibration problem of MEE plates under the framework of HSDT. The effect of the elastic foundation on the vibrations of MEE plates were analyzed by Shooshtari and Razavi (2016). In hygrothermal environment, the ability of HSDT to consider coupling effects to evaluate the natural frequencies was thoroughly investigated by Vinyas and Kattimani (2018b). In addition, the influence of carbon nano-tubes (CNT) on the frequency response of MEE plates with the aid of HSDT was assessed through a FE formulation by Vinyas (2019a).

The rectangular/square plates when provided with skewed edges, the stiffness drastically increases due to the fact that the area decreases. This improves the frequency of the plate. In addition, skewed MEE structures can be aligned easily even in case of obstructions. Therefore, the skewed structures are more often seen in the applications such as and actuators, energy harvesting and active vibration control (Vinyas 2019b). The free vibration behaviour of skew MEE plate was discussed by Vinyas *et al*. (2019) through higher-order shear deformation theory.

The literature survey reveals that limited articles have been reported on assessing the vibration behaviour of MEE plate under the framework of HSDT. Further, to the best of author's knowledge, no work has been reported on estimating the natural frequencies of SMEE plate considering temperature-moisture dependent elastic stiffness coefficients. In this regard, this work makes the first attempt by deriving a FE formulation with the aid of Hamilton's principle. The governing equations of motion are solved by incorporating Hamilton's principle. A special emphasize has been made on assessing the influence of skew angle of MEE plate. Further, the individual effect as well as the significant combination of temperature and moisture dependent empirical constants on the vibration frequencies of SMEE plate has been investigated. The obtained results are compared with the previously published literature to validate its credibility to yield close results as that of 3D thick plate solution as well. The possible limitation of this FE model may be associated with the large deflection free vibration of thick plates based on the 3D theory.

2. Materials and methods

Eqs. 1(a)-1(c) illustrate the constitutive equations of MEE displaying inter-coupling among elastic, electric and magnetic phases (Vinyas and Kattimani 2017a)

$$\{\sigma^n\} = \left[\tilde{C}^n\right]\{\varepsilon^n\} - [\tilde{e}^n]\{E^n\} - [\tilde{q}^n]\{H^n\} - [\tilde{\alpha}^n]\Delta T - \left[\tilde{\beta}^n\right]\Delta m \quad (1)$$

$$\{D^n\} = [\tilde{e}^n]\{\varepsilon^n\} - [\tilde{\eta}^n]\{E^n\} - [\tilde{m}^n]\{H^n\} - [\tilde{p}^n]\Delta T - [\tilde{\chi}^n]\Delta m \quad (2)$$

$$\{B\} = [\tilde{q}^n]\{\varepsilon^n\} - [\tilde{m}^n]\{E^n\} - [\tilde{\mu}^n]\{H^n\} - \left[\tilde{\lambda}^n\right]\Delta T - \left[\tilde{\zeta}^n\right]\Delta m \quad (3)$$

The nomenclature of the various material property matrices and vectors appearing in Eqs. 1(a)-1(c) are explicitly illustrated in the Appendix. Since, the present analysis considers plane stress state, the reduced elastic stiffness coefficients are used as follows

$$\tilde{C}_{11} = C_{11} - \frac{{C_{13}}^2}{C_{33}} \; ; \; \tilde{C}_{12} = C_{12} - \frac{C_{13}C_{23}}{C_{33}} \; ; \; \tilde{C}_{22} = C_{22} - \frac{{C_{23}}^2}{C_{33}} \; ; \; \tilde{C}_{44} = C_{44} \; ; \; \tilde{C}_{55} = C_{55} \; ; \; \tilde{C}_{66} = C_{66}$$
$$\tilde{e}_{31} = e_{31} - \frac{C_{13}e_{33}}{C_{33}} \; ; \; \tilde{e}_{32} = e_{32} - \frac{C_{23}e_{33}}{C_{33}} \; ; \; \tilde{e}_{15} = e_{15} \; ; \; \tilde{e}_{24} = e_{24} \; ;$$
$$\tilde{q}_{31} = q_{31} - \frac{C_{13}q_{33}}{C_{33}} \; ; \tilde{q}_{32} = q_{32} - \frac{C_{23}q_{33}}{C_{33}} \; ; \tilde{q}_{15} = q_{15} \; ; \; \tilde{q}_{24} = q_{24} \; ;$$
$$\tilde{\eta}_{11} = \eta_{11} \; ; \; \tilde{\eta}_{22} = \eta_{22}; \; \tilde{\eta}_{33} = \eta_{33} + \frac{{e^2}_{33}}{C_{33}} \; ; \tag{4}$$
$$\tilde{m}_{11} = m_{11} \; ; \; \tilde{m}_{22} = m_{22}; \; \tilde{m}_{33} = m_{33} + \frac{e_{33}q_{33}}{C_{33}} \; ; \tilde{\alpha}_1 = \alpha_1 - \frac{C_{13}\alpha_3}{C_{33}} \; ; \; \tilde{\alpha}_2 = \alpha_2 - \frac{C_{23}\alpha_3}{C_{33}} \; ;$$
$$\tilde{\beta}_1 = \beta_1 - \frac{C_{13}\beta_3}{C_{33}}; \; \tilde{\beta}_2 = \beta_2 - \frac{C_{23}\beta_3}{C_{33}}; \; \tilde{\zeta}_1 = \zeta_1 \; ; \; \tilde{\zeta}_2 = \zeta_2 \; ; \; \tilde{\zeta}_3 = \zeta_3 + \frac{q_{33}\beta_{33}}{C_{33}}$$
$$\tilde{p}_1 = p_1 \; ; \; \tilde{p}_2 = p_2 \; ; \; \tilde{p}_3 = p_3 + \frac{e_{33}\alpha_{33}}{C_{33}} \; ; \; \tilde{\lambda}_1 = \lambda_1 \; ; \; \tilde{\lambda}_2 = \lambda_2 \; ; \; \tilde{\lambda}_3 = \lambda_3 + \frac{q_{33}\alpha_{33}}{C_{33}}$$

2.1 Temperature and Moisture dependent material properties

The present analysis considers that the elastic stiffness coefficient is dependent on the temperature gradient ΔT (in Kelvin, K) and moisture concentration Δm (in %) through the empirical constants α^*(temperature dependent) and β^* (moisture dependent) as follows (Akbarzadeh and Chen 2012)

$$C = C_0(1 + \alpha^*\Delta T + \beta^*\Delta m) \tag{5}$$

in which, C_0 denotes the temperature and moisture independent elastic stiffness matrix. The significant empirical constants are obtained by evaluating the mechanical response of composite in hygrothermal environment experimentally, followed by fitting the mathematical relation (Youssef 2005, Adams and Miller 1997). Meanwhile, the empirical constants are assumed not to vary in any direction.

2.2 Methodology

This study is structured according to the stages that involved the development of the finite element based on Reddy's TSDT. Therefore, in this section one starts by considering the displacement and strain fields associated to this theory, which is then followed by the corresponding finite element formulation. Considering that the plates that will be analyzed are made of temperature and moisture dependent magneto-electro-elastic materials, the corresponding constitutive relations are considered in the equation of motion constitution, as well as the necessary transformations to deal with the plates' geometrical skewness.

2.3 Problem description

The present study considers a three layered rectangular (Fig. 1(a)) and SMEE plates (Figs. 1(b) and 1(c)) having a, b and h as dimensions of length, breadth and thickness (Fig. 1). The geometrical skewness of the plate is denoted by α. .The SMEE plate with first and third layers made of piezoelectric (B) and the middle layer made of piezomagnetic (F) material forms BFB stacking sequence. Meanwhile, replacing the piezoelectric and piezomagnetic layers in BFB stacking sequence forms FBF stacking sequence.

2.4 Reddy's third order shear deformation theory

The plate kinematics follows Reddy's third order shear deformation theory (RTSDT) according to which the displacement components u, v and w can be represented as (Reddy 1997)

$$u = u_0 + z\theta_x - \frac{4}{3h^2}z^3\left(\theta_x + \frac{\partial w_0}{\partial x}\right)$$
$$v = v_0 + z\theta_y - \frac{4}{3h^2}z^3\left(\theta_y + \frac{\partial w_0}{\partial y}\right) \tag{6}$$
$$w = w_0$$

in which, the midplane displacements along x, y, and z-axes are denoted asu_0, v_0, and w_0, respectively. Meanwhile, the rotations of the normal in the xz plane and yz plane are shown as θ_x and θ_y, respectively. Further, z = 0 acts as a mid-plane.

Categorizing into bending and shear strains, the strain components can be illustrated as follows

$$\{\varepsilon_b\} = \begin{Bmatrix}\varepsilon_x\\ \varepsilon_y\\ \gamma_{xy}\end{Bmatrix} = \begin{bmatrix}\frac{\partial}{\partial x} & 0 & 0\\ 0 & \frac{\partial}{\partial y} & 0\\ \frac{\partial}{\partial y} & \frac{\partial}{\partial x} & 0\end{bmatrix}\begin{Bmatrix}u_0\\ v_0\\ w_0\end{Bmatrix} + \left(z + c_1 z^3\right)\begin{bmatrix}\frac{\partial}{\partial x} & 0\\ 0 & \frac{\partial}{\partial y}\\ \frac{\partial}{\partial y} & \frac{\partial}{\partial x}\end{bmatrix}\begin{Bmatrix}\theta_x\\ \theta_y\end{Bmatrix} + c_1 z^3\begin{bmatrix}\frac{\partial}{\partial x} & 0\\ 0 & \frac{\partial}{\partial y}\\ \frac{\partial}{\partial y} & \frac{\partial}{\partial x}\end{bmatrix}\begin{Bmatrix}\kappa_x\\ \kappa_y\end{Bmatrix} \tag{7}$$

$$\{\varepsilon_b\} = [B_{tb}]\{d_t^e\} + z[B_{rb}]\{d_r^e\} + c_1 z^3[B_{rb}]\{d_r^e\} + c_1 z^3[B_{rb}]\{d_{r*}^e\} \tag{8}$$

where

$$\kappa_x = \frac{\partial w_0}{\partial x}, \kappa_y = \frac{\partial w_0}{\partial y}, \; c_1 = -\frac{4}{3h^2}, \; \{d_t^e\} = \begin{Bmatrix}u_0\\ v_0\\ w_0\end{Bmatrix}, \; \{d_r^e\} = \begin{Bmatrix}\theta_x\\ \theta_y\end{Bmatrix}, \; \{d_{r*}^e\} = \begin{Bmatrix}\kappa_x\\ \kappa_y\end{Bmatrix} \tag{9}$$

$$\left[B_{tb}\right]=\begin{bmatrix}\dfrac{\partial}{\partial x} & 0 & 0\\ 0 & \dfrac{\partial}{\partial y} & 0\\ \dfrac{\partial}{\partial y} & \dfrac{\partial}{\partial x} & 0\end{bmatrix},\ \left[B_{rb}\right]=\begin{bmatrix}\dfrac{\partial}{\partial x} & 0\\ 0 & \dfrac{\partial}{\partial y}\\ \dfrac{\partial}{\partial y} & \dfrac{\partial}{\partial x}\end{bmatrix} \tag{10}$$

The shear strains can be expressed as follows

$$\{\varepsilon_s\}=\begin{Bmatrix}\gamma_{xz}\\ \gamma_{yz}\end{Bmatrix}=\begin{bmatrix}0 & 0 & \dfrac{\partial}{\partial x}\\ 0 & 0 & \dfrac{\partial}{\partial y}\end{bmatrix}\begin{Bmatrix}u_0\\ v_0\\ w_0\end{Bmatrix}+\begin{bmatrix}1 & 0\\ 0 & 1\end{bmatrix}\begin{Bmatrix}\theta_x\\ \theta_y\end{Bmatrix}+c_2z^2\begin{bmatrix}1 & 0\\ 0 & 1\end{bmatrix}\begin{Bmatrix}\theta_x\\ \theta_y\end{Bmatrix}+\begin{bmatrix}1 & 0\\ 0 & 1\end{bmatrix}\begin{Bmatrix}\kappa_x\\ \kappa_y\end{Bmatrix} \tag{11}$$

$$\{\varepsilon_s\}=\left[B_{ts}\right]\left\{d_t^e\right\}+\left[B_{rs}\right]\left\{d_r^e\right\}+c_2z^2\left[B_{rs}\right]\left\{d_r^e\right\}+c_2z^2\left[B_{rs}\right]\left\{d_{r*}^e\right\} \tag{12}$$

in which

$$c_2=-\frac{4}{h^2},\ \left[B_{ts}\right]=\begin{bmatrix}0 & 0 & \dfrac{\partial}{\partial x}\\ 0 & 0 & \dfrac{\partial}{\partial y}\end{bmatrix},\ \left[B_{rs}\right]=\begin{bmatrix}1 & 0\\ 0 & 1\end{bmatrix} \tag{13}$$

In the Eqs. (8)- (11), $[B_{tb}]$, $[B_{rb}]$, $[B_{ts}]$and $[B_{rs}]$ are the strain-displacement matrices. Meanwhile, $\{d_t\}=\{u_0 \quad v_0 \quad w_0\}^T$, $\{d_r\}=\{\theta_x \quad \theta_y\}^T$ and $\{d_{r*}\}=\{\kappa_x \quad \kappa_y\}^T$ are the translational, rotational and higher-order displacement vector, respectively.

2.5 Finite element formulation

The details regarding the derivation of finite element (FE) in association with the RTSDT has been presented in this section. An eight noded isoparametric element is used to develop the FE model. Each node of the element accommodates nine degrees of freedom related to$\{d_t\}$, $\{d_r\}$,$\{d_{r*}\}$, electric potential (ϕ) and magnetic potential (ψ). The generalized translational displacement vector and rotational vector associated with the i^{th}(i =1, 2, 3…8) node of the element can be represented as

$$\begin{aligned}\left\{d_{ti}\right\}&=\left[u_i \ \ v_i \ \ w_i\right]^T,\ \left\{d_{ri}\right\}=\left[\theta_x \quad \theta_y\right]^T\\ \left\{d_{r*i}\right\}&=\left[\kappa_x \quad \kappa_y\right]^T\end{aligned} \tag{14}$$

$$\begin{aligned}\left\{d_t\right\}&=\left[N_t\right]\left\{d_t^e\right\},\left\{d_r\right\}=\left[N_r\right]\left\{d_r^e\right\},\\ \left\{d_{r*}\right\}&=\left[N_{r*}\right]\left\{d_{r*}^e\right\},\left\{\phi\right\}=\left[N_\phi\right]\ \left\{\phi^e\right\}\\ \left\{\psi\right\}&=\left[N_\psi\right]\ \left\{\psi^e\right\}\end{aligned} \tag{15}$$

where, $[N_t]$, $[N_r]$,$[N_{r*}]$,$[N_\phi]$ and$[N_\psi]$ are shape function matrices, respectively.

Assuming the quasi-staticelectro-magnetic behavior, the electric field (E) and magnetic field (H) can be related to scalar gradients of its potential as follows

$$\left\{E\right\}=-\phi_{,i}=\left[B_\phi\right]\left\{\phi^e\right\} \tag{16}$$

$$\left\{H\right\}=-\psi_{,i}=\left[B_\psi\right]\left\{\psi^e\right\} \tag{17}$$

in which, $i = x, y$ and z.

2.6 Equation of motion

The expression of Hamilton's principle for SMEE plate can be given as follows

$$E=\frac{1}{2}\sum_{n=1}^{N}\int_{\Omega^n}\delta\{\varepsilon_b\}^T\{\sigma_b\}d\Omega^n+\frac{1}{2}\sum_{n=1}^{N}\int_{\Omega k}\delta\{\varepsilon_s\}^T\{\sigma_s\}d\Omega^n- \tag{18}$$

$$\frac{1}{2}\sum_{n=1}^{N}\int_{\Omega^n}\delta\{E\}^T\{D\}d\Omega^n-\frac{1}{2}\sum_{n=1}^{N}\int_{\Omega^n}\delta\{H\}^T\{B\}\ \Omega^n+\int_{\Omega^n}\delta\{d_t\}\rho\{\ddot{d}_t\}d\Omega^n$$

In Eq. (18), the layer number is shown as n and the volume of the n^{th} layer is depicted as Ω^n. In the present analysis, the effect of the mechanical load vector$\{F_m^e\}^T$, the electric load vector $\left\{F_\phi^e\right\}^T$ and magnetic load vector $\left\{F_\psi^e\right\}^T$ are neglected. Further, bifurcating the terms based on the coefficients of $\{d_t^e\}^T$,$\{d_r^e\}^T$, $\{d_{r*}^e\}^T$, $\{\phi^e\}^T$ and $\{\psi^e\}^T$,we obtain the equations of motion as follows

$$\begin{aligned}[M_{tt}]\{\ddot{d}_t\}+[K_{tt}]\{d_t\}+[K_{tr}]\{d_r\}+[K_{tr*}]\{d_{r*}\}+[K_{t\phi}]\{\phi\}+[K_{t\psi}]\{\psi\}=0\\ [K_{rt}]\{d_t\}+[K_{rr}]\{d_r\}+[K_{rr*}]\{d_{r*}\}+[K_{r\phi}]\{\phi\}+[K_{r\psi}]\{\psi\}=0\\ [K_{r*t}]\{d_t\}+[K_{r*r}]\{d_r\}+[K_{r*r*}]\{d_{r*}\}+[K_{r*\phi}]\{\phi\}+[K_{r*\psi}]\{\psi\}=0\\ [K_{\phi t}]\{d_t\}+[K_{\phi r}]\{d_r\}+[K_{\phi r*}]\{d_{r*}\}+[K_{\phi\phi}]\{\phi\}+[K_{\phi\psi}]\{\psi\}=0\\ [K_{\psi t}]\{d_t\}+[K_{\psi r}]\{d_r\}+[K_{\psi r*}]\{d_{r*}\}+[K_{\psi\phi}]\{\phi\}+[K_{\psi\psi}]\{\psi\}=0\end{aligned} \tag{19}$$

The skew transformations are applied by imposing transformed boundary conditions along *x'-*, *y'-* and *z'-* directions, to the degrees of freedom of the points lying on the skew edges as follows

$$\left\{d_t\right\}=\left[T_t\right]\left\{d_t^1\right\}\ ;\ \left\{d_r\right\}=\left[T_r\right]\left\{d_r^1\right\}\ ;\ \left\{d_{r*}\right\}=\left[T_{r*}\right]\left\{d_{r*}^1\right\} \tag{20}$$

$\left\{d_t^1\right\}$, and by $\left\{d_r^1\right\}$, $\left\{d_{r*}^1\right\}$ denotes skew transformed translational, rotational and higher order degrees of freedom, respectively. Further, the transformation matrices$[T_t]$, $[T_r]$ and $[T_{r*}]$ implemented at each node can be shown as follows

$$\left[T_t\right]=\begin{bmatrix}\cos\alpha & \sin\alpha & 0\\ -\sin\alpha & \cos\alpha & 0\\ 0 & 0 & 1\end{bmatrix}\ ;\ \left[T_r\right]=\left[T_{r*}\right]=\begin{bmatrix}\cos\alpha & \sin\alpha\\ -\sin\alpha & \cos\alpha\end{bmatrix} \tag{21}$$

Similarly, the transformed stiffness and mass matrices can be illustrated as follows

$$\left[\overline{K_{tt}^e}\right]=\left[T_1\right]^T\left[K_{tt}^e\right]\left[T_1\right]\ ;\ \left[\overline{K_{tr}^e}\right]=\left[T_1\right]^T\left[K_{tr}^e\right]\left[T_2\right]\ ;\ \left[\overline{K_{tr*}^e}\right]=\left[T_1\right]^T\left[K_{tr*}^e\right]\left[T_2\right] \tag{22}$$

$$\left[\overline{K_{rr}^e}\right]=\left[T_2\right]^T\left[K_{rr}^e\right]\left[T_2\right]\ ;\ \left[\overline{K_{rr*}^e}\right]=\left[T_2\right]^T\left[K_{rr*}^e\right]\left[T_2\right]\ ;\ \left[\overline{K_{r*r*}^e}\right]=\left[T_2\right]^T\left[K_{r*r*}^e\right]\left[T_2\right]$$

$$\left[\overline{M^e}\right]=\left[T_1\right]^T\left[M^e\right]\left[T_1\right]$$

Table 1 Material properties corresponding to different volume fraction V_f of $BaTiO_3 - CoFe_2O_4$ (Vinyas and Kattimani 2017b)

Material property	Material Constants	0 V_f	0.2 V_f	0.4 V_f	0.5 V_f	0.6 V_f	0.8 V_f	1 V_f
Elastic Constants (GPa)	$C_{11}=C_{22}$	286	250	225	220	200	175	166
	C_{12}	173	146	125	120	110	100	77
	$C_{13}=C_{23}$	170	145	125	120	110	100	78
	C_{33}	269.5	240	220	215	190	170	162
	$C_{44}=C_{55}$	45.3	45	45	45	45	50	43
	C_{66}	56.5	52	50	50	45	37.5	44.5
Piezoelectric constants (C/m^2)	e_{31}	0	-2	-3	-3.5	-3.5	-4	-4.4
	e_{33}	0	4	7	9.0	11	14	18.6
	e_{15}	0	0	0	0	0	0	11.6
Dielectric constant ($10^{-9}\,C^2/Nm^2$)	$\varepsilon_{11}=\varepsilon_{22}$	0.08	0.33	0.8	0.85	0.9	1	11.2
	ε_{33}	0.093	2.5	5	6.3	7.5	10	12.6
Magnetic permeability ($10^{-4}\,Ns^2/C^2$)	$\mu_{11}=\mu_{22}$	-5.9	-3.9	-2.5	-2.0	-1.5	-0.8	0.05
	μ_{33}	1.57	1.33	1	0.9	0.75	0.5	0.1
Piezomagnetic constants (N/Am)	q_{31}	580	410	300	350	200	100	0
	q_{33}	700	550	380	320	260	120	0
	q_{15}	560	340	220	200	180	80	0
Magneto-electric constant (10^{-12}Ns/VC)	$m_{11}=m_{22}$	0	2.8	4.8	5.5	6	6.8	0
	m_{33}	0	2000	2750	2600	2500	1500	0
Density (kg/m^3)	ρ	5300	5400	5500	5550	5600	5700	5800

where $\left[T_1\right]$ and $\left[T_2\right]$ are banded matrices containing the matrices present in Eq. (21) along the main diagonals, respectively. Finally, Eq. (19) can be condensed to a more generalized form as follows

$$\left[M_{eq}\right]\left\{\ddot{d}_t\right\}+\left[K_{eq}\right]\left\{d_t\right\}=0 \tag{23}$$

where, $\left[K_{eq}\right]$and $\left[M_{eq}\right]$is the equivalent stiffness and mass matrix.

The boundary conditions at the nodes laying on the skew edges can be expressed along the transformed axes as follows

Clamped edge (C):

$$u^1=v^1=w^1=\theta_x^1=\theta_y^1=\kappa_x^1=\kappa_y^1=\phi=\psi=0$$

Simply supported edge (S): (24)

$$u^1=\theta_x^1=\kappa_x^1\neq 0; v^1=w^1=\phi=\psi=0 \quad \text{at } x^1=0,\ a$$

$$v^1=\theta_y^1=\kappa_y^1\neq 0; u^1=w^1=\phi=\psi=0 \quad \text{at } y^1=0,b$$

3. Results and discussion

In this section, the natural frequency characteristics of SMEE have been assessed with the aid of FE formulation derived, considering temperature-moisture dependent elastic stiffness coefficients. The geometrical dimensions of the plate considered are $a = b = 1$m and thickness $h = 0.3$ m. The METE material properties tabulated in Table 1 are considered in this analysis. A mesh size of 10×10 which yields a converged result has been adopted in the present work. Analogously, the verification of the present FE model is carried out by comparing the results with the previously published literature. The usefulness of the FE formulation derived is able to employ them in place of more general three-dimensional analyses to obtain much accurate results. The 3D analyses require higher computational time and involve greater numerical round-off error difficulties. Further, it eliminates the over corrections in frequencies caused by first order theory for moderate and large thickness. In this regard, to prove the credibility of the proposed formulation to yield accurate results against the existing 3D thick plate solution, the problem of layered thick MEE plates as considered by Chen *et al.* (2014) is resolved through the present formulation. From Table 2 it is affirmed that the proposed FE formulation results in an accurate prediction of coupled natural frequency of plate up-to a very low length/thickness ratio of 5 (thick plates).

3.1 Effect of temperature-moisture dependent empirical constants

The influence of temperature dependent empirical constant $\alpha^*$and moisture dependent empirical constant β^* on the natural frequency of MEE plate is evaluated using FE formulation. The temperature and moisture dependent elastic stiffness coefficient C as depicted in Eq. (5) is considered for evaluation. Further, in the present analysis, MEE plate with BFB stacking sequence (the term '*B*' and '*F*' corresponds to the pure piezoelectric and pure piezomagnetic phases, respectively) subjected to the temperature difference of 10 *K* and a moisture concentration of 0.5 has been considered. The evaluation is carried out for SSSS and CCCC boundary conditions. For the sake of brevity, only the variation of the

Table 2 Verification of the present FE formulation ($a/h = 5$)

Stacking Sequence	Mode No.	Non-Dimensional Frequency		% Error
		Chen *et al.* (2014)	Present	
BBB	1	1.7823	1.7871	0.2673
	2	2.9492	2.9534	0.1433
	3	2.9492	2.9537	0.1512
FFF	1	1.3674	1.3736	0.4518
	2	2.2318	2.2404	0.3841
	3	2.2318	2.2404	0.3841
BFB	1	1.3434	1.3482	0.3601
	2	2.2199	2.2279	0.3597
	3	2.2199	2.2279	0.3597
FBF	1	1.4463	1.4346	-0.8109
	2	2.3602	2.3390	-0.8979
	3	2.3602	2.3392	-0.8905

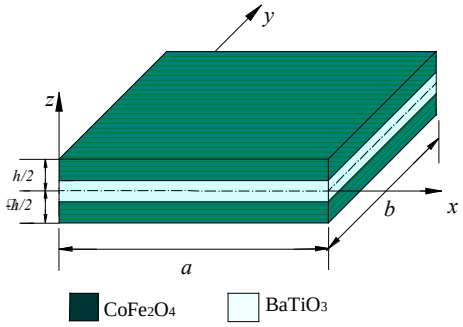

(a) Rectangular MEE plate

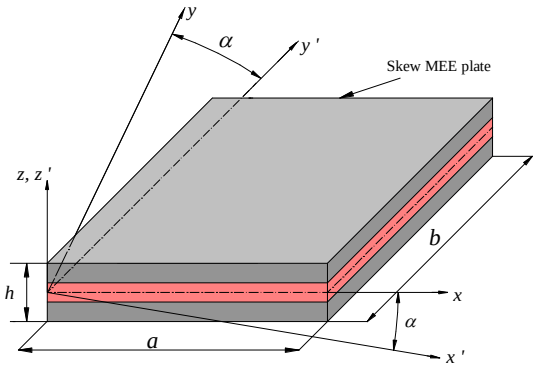

(b) Skew MEE plate

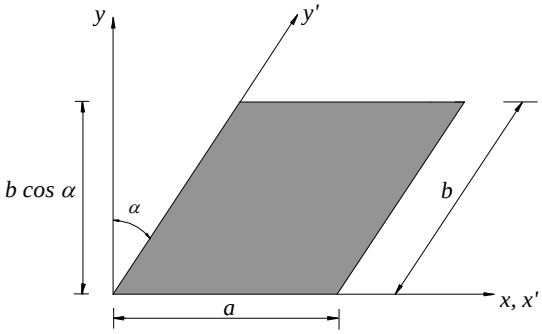

(c) Skew Transformation

Fig. 1 Magneto-electro-elastic plate geometry

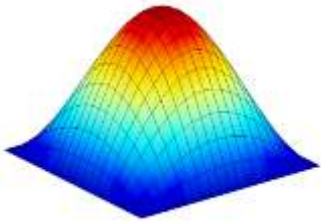

(a) 1st Mode

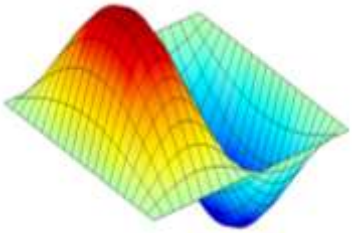

(b) 2nd Mode

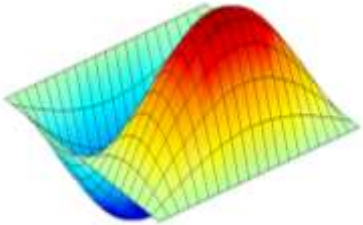

(c) 3rd Mode

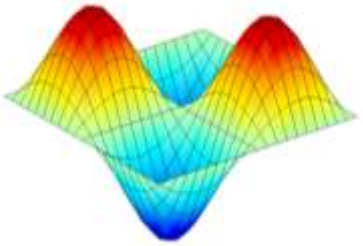

(d) 4th Mode

Fig. 2 Mode shapes of MEE plate (CCCC boundary condition)

Table 3 Effect of $\alpha^*$and β^* on the natural frequency of MEE plate

BFB stacking sequence, ΔT= *10 K;* Δm=0.5								
	SSSS				CCCC			
α^*	β^* = 0.5	β^* = 1.0	β^* = 1.5	β^*= 2.0	β^* = 0.5	β^* = 1.0	β^* = 1.5	β^*= 2.0
0.5	0.3249	0.3314	0.3377	0.3439	0.4324	0.4410	0.4494	0.4576
	0.5848	0.5964	0.6078	0.6189	0.9176	0.9358	0.9536	0.9712
	0.6431	0.6558	0.6683	0.6806	0.9176	0.9358	0.9536	0.9712
1.0	0.4359	0.4408	0.4455	0.4502	0.5802	0.5866	0.5929	0.5992
	0.7846	0.7933	0.8019	0.8103	1.2313	1.2449	1.2584	1.2717
	0.8628	0.8723	0.8818	0.8911	1.2313	1.2449	1.2584	1.2717
1.5	0.5239	0.5280	0.5319	0.5359	0.6973	0.7026	0.7079	0.7132
	0.9430	0.9502	0.9574	0.9645	1.480	1.4913	1.5026	1.5137
	1.0369	1.0449	1.0528	1.0606	1.480	1.4913	1.5026	1.5137
2.0	0.5991	0.6027	0.6062	0.6096	0.7974	0.8020	0.8067	0.8113
	1.0783	1.0847	1.0910	1.0971	1.6924	1.7024	1.7122	1.7221
	1.1858	1.1927	1.1997	1.2055	1.6924	1.7024	1.7122	1.7221

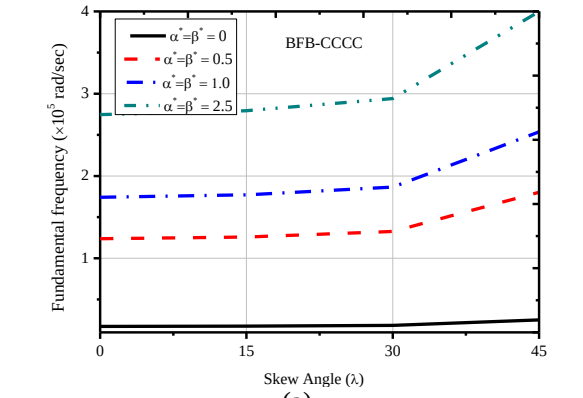

(a)

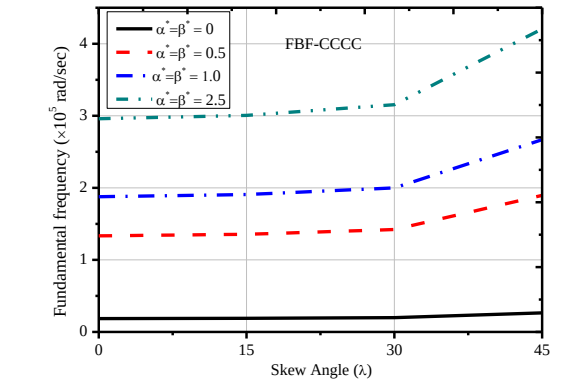

(b)

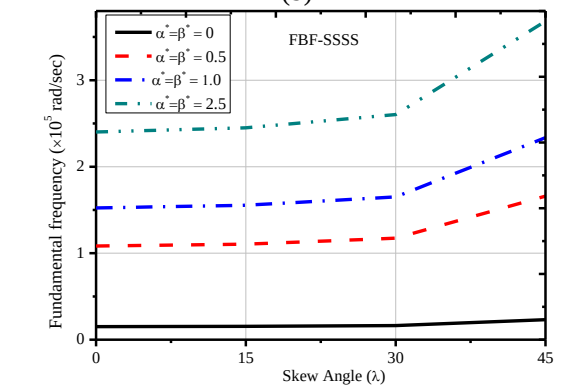

(c)

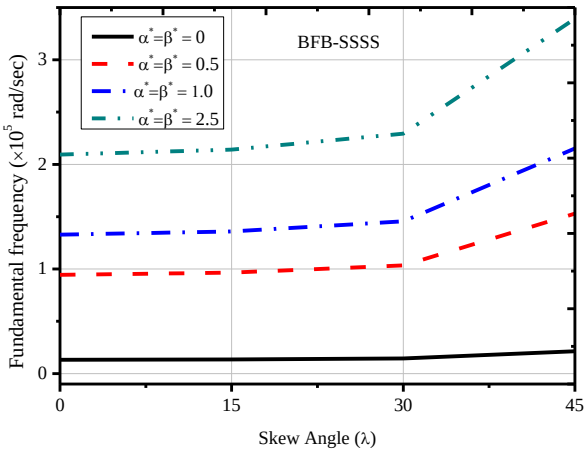

(d)

Fig. 3 Effect of skew angle on the SMEE plates with different empirical constants

Table 4 Effect of skew angle on MEE plate with different empirical constants (BFB; ΔT = 100 K; Δm = 1)

Skew Angle	Natural frequency (× 10^5 rad sec^{-1})					
	SSSS			CCCC		
	Empirical constants $\alpha^* = \beta^*$					
	0.5	1	2.5	0.5	1	2.5
$\lambda = 0^0$	0.9439	1.3284	2.0941	1.2377	1.7418	2.7459
	1.201	1.6902	2.6645	2.0647	2.9058	4.5809
	1.201	1.6902	2.6645	2.0647	2.9058	4.5809
$\lambda = 10^0$	0.9655	1.3587	2.142	1.2588	1.7716	2.7929
	1.2163	1.7117	2.6984	2.0357	2.865	4.5166
	1.2232	1.7215	2.7139	2.158	3.0371	4.7879
$\lambda = 20^0$	1.0339	1.4551	2.294	1.3257	1.3257	2.9413
	1.2641	1.7791	2.8046	2.0697	2.0697	4.5919
	1.2955	1.8231	2.8742	2.3275	2.3275	5.1639
$\lambda = 45^0$	1.5294	2.1524	3.3932	1.8023	2.5364	0.3999
	1.5945	2.2439	3.5375	2.5354	3.5681	0.5625
	1.8492	2.6024	4.1026	2.9108	4.0965	0.6458

Table 5 Effect of skew angle on MEE plate with different empirical constants (FBF; ΔT = 100 K; Δm = 1)

Skew Angle	Natural frequency (× 10^5 rad sec^{-1})					
	SSSS			CCCC		
	Empirical constants $\alpha^* = \beta^*$					
	0.5	1	2.5	0.5	1	2.5
$\lambda = 0^0$	1.0825	1.0825	2.4017	1.334	1.8773	2.9596
	1.2495	1.2495	2.7722	2.1834	3.0728	4.8442
	1.2495	1.2495	2.7722	2.1834	3.0728	4.8442
$\lambda = 10^0$	1.1043	1.5541	2.45	1.355	1.907	3.0063
	1.2655	1.7809	2.8076	2.1532	3.0302	4.7771
	1.2731	1.7917	2.8245	2.2783	3.2063	5.0547
$\lambda = 20^0$	1.1733	1.6512	2.6031	1.4215	2.0005	3.1538
	1.3155	1.8513	2.9186	2.186	3.0764	4.8498
	1.3498	1.8997	2.9948	2.45	3.4479	5.4355
$\lambda = 45^0$	1.6601	2.3363	3.6831	1.8956	2.6677	0.4206
	1.6689	2.3487	3.7027	2.6474	3.7258	0.5874
	1.9404	2.7307	4.3049	3.0975	4.3592	0.6872

first natural frequency is depicted in this section. It can be noticed from Table 3 that for a given α^*, the natural frequency increases for the higher values of β^*. Figs. 2(a)-2(d) illustrate the first four mode shapes of MEE plate subjected to ΔT= *10* K and Δm=0.5. The empirical constants correspond to α^*= β^* = 0.5.

3.2 Effect of skew angle

The influence of skew angle on the coupled frequency of SMEE plates has been analyzed. The results plotted in Figs. 3(a)-3(d) suggest that with the increase in the skew angle of the SMEE plate, the natural frequencies increases. It may be due to the fact that the area of the plate decreases leading to improved stiffness of the plate. The mode shapes

Mode No.	Skew Angle (α)		
	15°	30°	45°
1	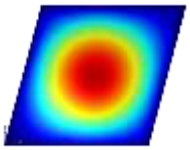	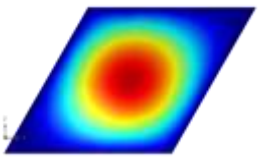	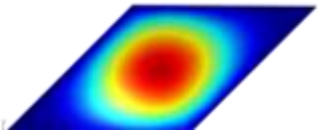
2	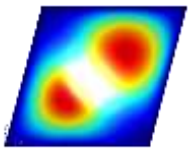	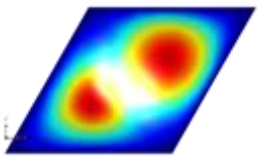	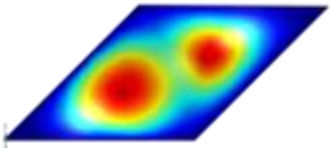
3	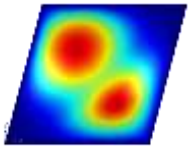	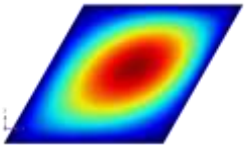	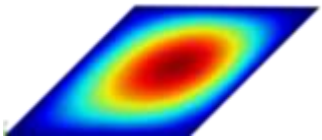
4	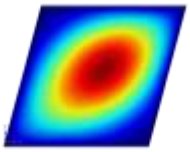	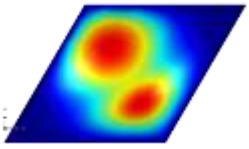	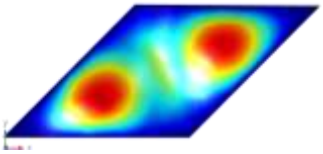
5	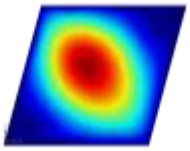	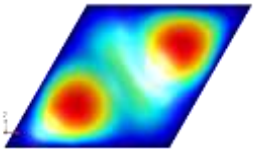	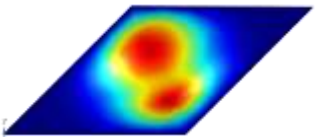
6	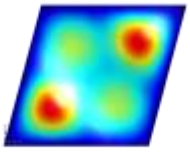	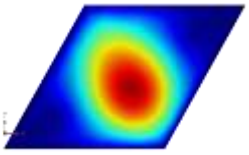	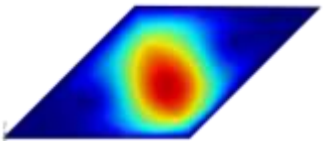

Fig. 4 Mode shapes of SMEE plates-BFB stacking sequence

corresponding to the different skew angle is illustrated in Fig. 4. Further, it also witnessed that a drastic change in the frequency appears when the skew angle changes from 30 to 45 degree. This holds good for all the temperature and moisture dependent empirical constants adopted for the analysis, as elucidated in Tables 4 and 5. In addition, it is also witnessed here that the higher empirical constants yields higher natural frequency.

The analysis is extended to compare the natural frequency of SMEE plate considering the effect of temperature and moisture dependent elastic stiffness coefficients with that of temperature and moisture independent elastic stiffness coefficients. The results tabulated in Table 6 reveals that for different stacking sequences and boundary conditions, the natural frequencies show a prominent effect when the elastic stiffness coefficients are considered to be dependent on the external temperature and moisture fields. In addition, the effect of skew angle is evaluated on the same grounds. The results reveal that the discrepancy between the natural frequencies of SMEE plate with and without considering temperature and moisture dependent elastic stiffness coefficients becomes more at the higher skew angle as depicted in Figs. 5(a)-5(d).

3.3 Effect of stacking sequences

For a unit change in the external thermal and moisture fields, the effect of stacking sequences on the first four natural frequencies of MEE plate with CCCC boundary

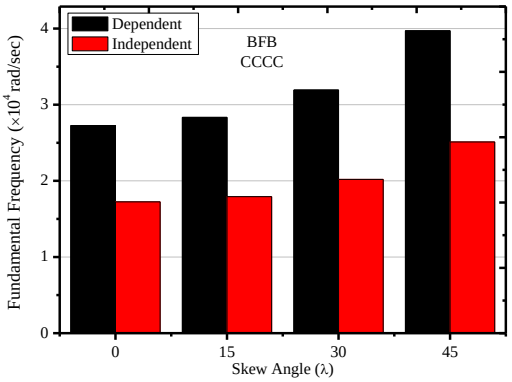

(a)

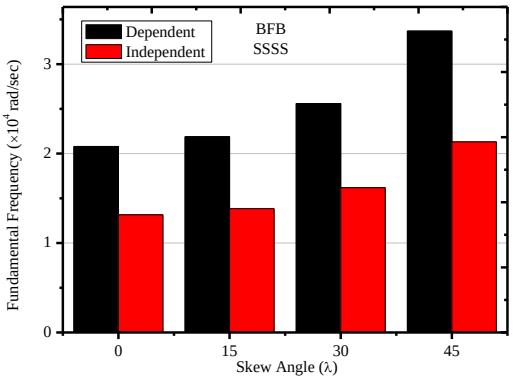

(b)

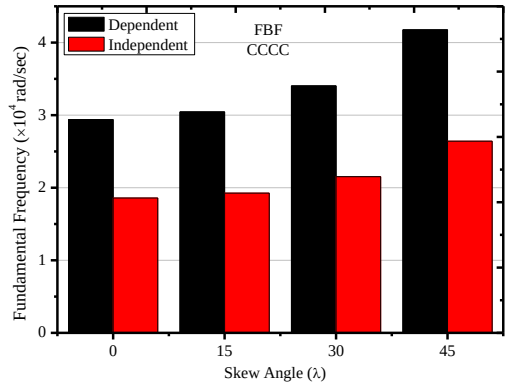

(c)

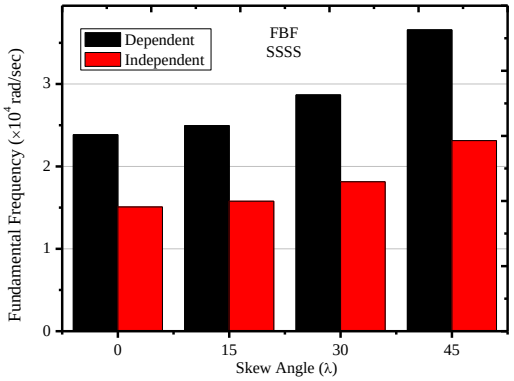

(d)

Fig. 5 Comparison of fundamental frequency of SMEE plate with tempereature-moisture dependent and independent material properties

Table 6 Comparison of the natural frequencies corresponding to temperature and moisture dependent and indep endent elastic stiffness coefficients with different boundary conditions

Stacking Sequence	Natural frequencies (10^4 rad/sec), $\alpha^* = \beta^* = 1$							
	SSSS		CCCC		CSCS		CFCF	
	ΔT and Δm							
	independent	dependent	independent	dependent	independent	dependent	independent	dependent
BFB	1.3191	2.2848	1.7297	2.9959	1.5208	2.6341	1.1668	2.0209
	2.3747	4.1131	3.6634	6.3549	2.8205	4.8852	2.2317	3.8654
	2.6198	4.5377	3.6634	6.3549	3.0905	5.3546	2.4934	4.3187
FBF	1.5129	2.6204	1.8643	3.2291	1.6713	2.8948	1.2624	2.1865
	2.4708	4.2796	3.9415	6.8369	2.9987	5.194	2.4671	4.2732
	2.8534	4.9415	3.9415	6.8369	3.2406	5.6144	2.6246	4.5459
BFFB	1.3406	2.3220	1.7445	3.0216	1.5372	2.6625	1.1774	2.0393
	2.4233	4.1972	3.8055	6.6012	2.8402	4.9193	2.2578	3.9106
	2.6444	4.5803	3.8055	6.6012	3.1671	5.4872	2.5088	4.3454
FBBF	1.4994	2.5971	1.8542	3.2113	1.6602	2.8755	1.255	2.1737
	2.4233	4.1972	3.8055	6.6012	2.983	5.1666	2.4482	4.2404
	2.8369	4.9137	3.8055	6.6012	3.1671	5.4872	2.6114	4.523
BBB	1.3036	2.2580	1.7105	2.9627	1.5037	2.6046	1.1542	1.9991
	2.2745	3.9396	3.3569	5.8245	2.7893	4.8313	2.2074	3.8233
	2.5904	4.4867	3.3569	5.8245	2.9248	5.0684	2.4666	4.2722
FFF	1.5278	2.6462	1.8841	3.263	1.6885	2.9245	1.2753	2.2088
	2.5634	4.4399	4.029	6.978	3.0308	5.2496	2.4914	4.3152
	2.8835	4.9943	4.1758	7.233	3.3802	5.8561	2.6522	4.5938

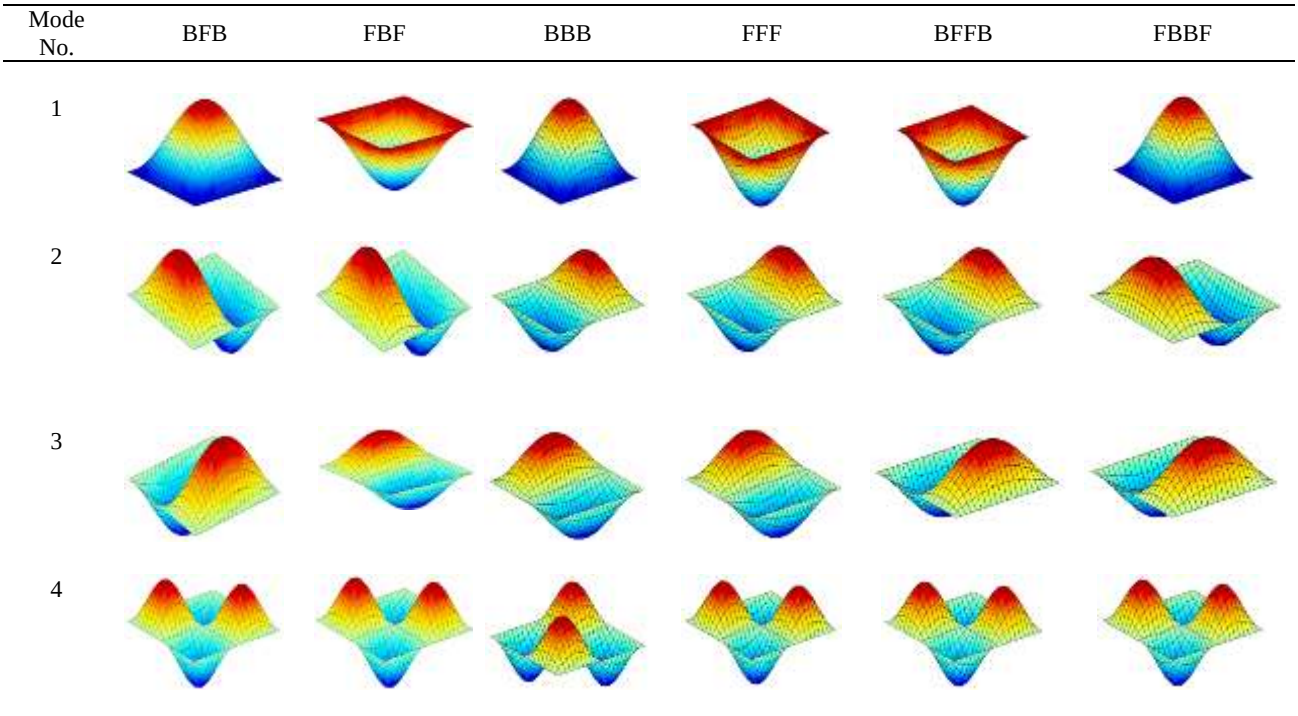

Fig. 6 Effect of stacking sequences on the mode shapes of MEE plates subjected to hygrothermal loads ($\Delta T = \Delta m = 1$)

Table 7 Effect of different combination of empirical constants on the fundamental frequency of SMEE plate (*ΔT= 10 K; Δm*=0.5; CCCC condition)

Skew Angle	Fundamental natural frequency (× 10^5 rad sec^{-1})								
		BFB				FBF			
	α^*	β^* = 0.5	β^* = 1.0	β^* = 1.5	β^*= 2.0	β^* = 0.5	β^* = 1.0	β^* = 1.5	β^*= 2.0
λ=0°	0.5	1.2377	1.2437	1.2496	1.2556	1.334	1.3404	1.3469	1.3533
	1.0	1.7375	1.7418	1.7461	1.7503	1.8727	1.8773	1.8819	1.8865
	1.5	2.1228	2.1263	2.1298	2.1333	2.288	2.2917	2.2955	2.2993
	2.0	2.4481	2.4512	2.4542	2.4572	2.6386	2.6419	2.6452	2.6484
λ=15°	0.5	1.2588	1.2649	1.271	1.277	1.355	1.3616	1.3681	1.3746
	1.0	1.7673	1.7716	1.776	1.7803	1.9023	1.907	1.9116	1.9163
	1.5	2.1591	2.1627	2.1662	2.1698	2.3241	2.3279	2.3317	2.3356
	2.0	2.49	2.4931	2.4962	2.4993	2.6803	2.6836	2.6869	2.6903
λ= 30°	0.5	1.3257	1.3321	1.3385	1.3449	1.4215	1.4284	1.4352	1.4421
	1.0	1.8611	1.8657	1.8703	1.8748	1.9956	2.0005	2.0054	2.0103
	1.5	2.2738	2.2775	2.2813	2.285	2.4381	2.4421	2.4461	2.4501
	2.0	2.6223	2.6255	2.6288	2.632	2.8118	2.8153	2.8188	2.8222
λ= 45°	0.5	1.8023	1.811	1.8197	1.8283	1.8956	1.9047	1.9139	1.923
	1.0	2.5302	2.5364	2.5426	2.5488	2.6611	2.6677	2.6742	2.6807
	1.5	3.0912	3.0962	3.1013	3.1064	3.2512	3.2565	3.2619	3.2672
	2.0	3.565	3.569	3.574	3.578	3.749	3.754	3.759	3.763

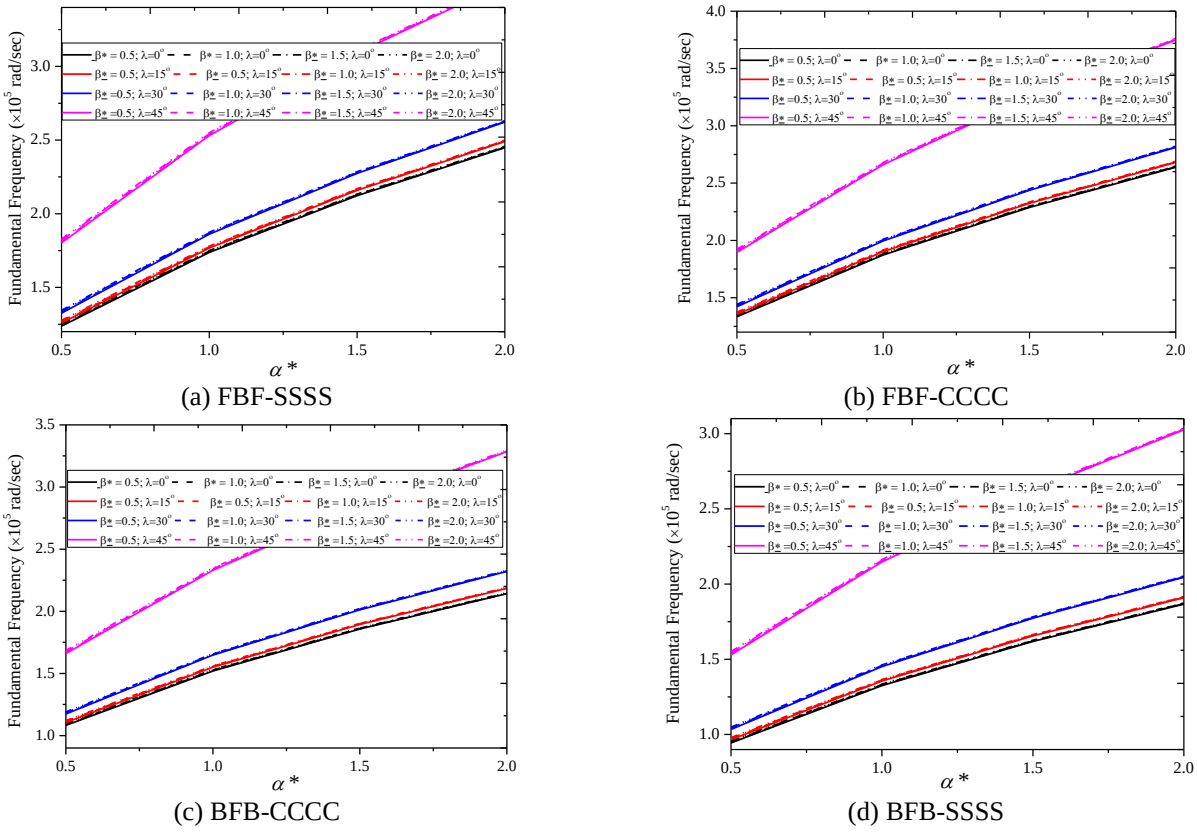

(a) FBF-SSSS (b) FBF-CCCC

(c) BFB-CCCC (d) BFB-SSSS

Fig. 7 Effect of different combination of empirical constants and skew angle on the fundamnetal frequency of SMEE plate

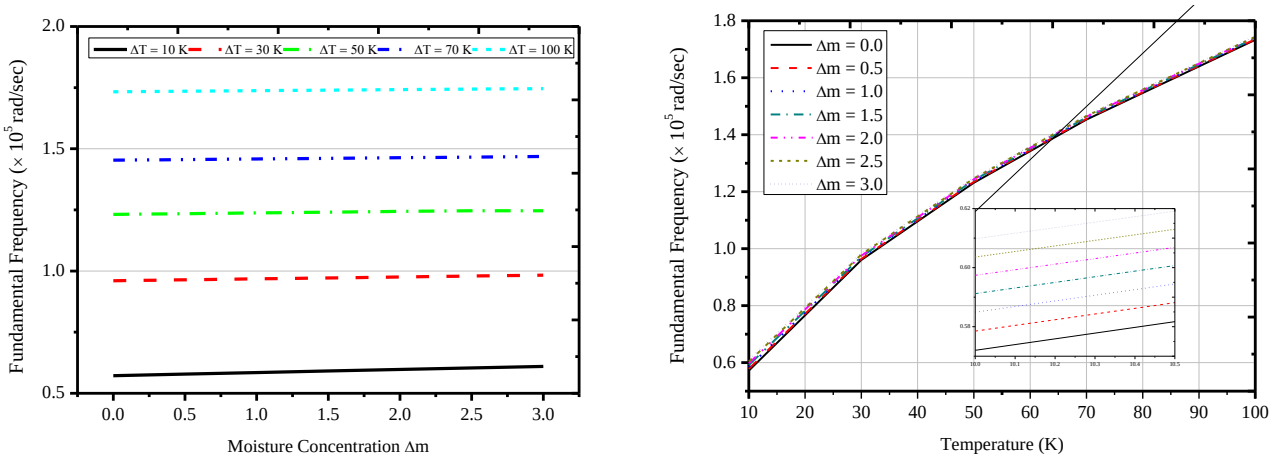

Fig. 8 Effect of (a) Δm at constant value of ΔT and (b)ΔT at constant value of Δm

condition is studied. It can be noticed from Table 6 that MEE pate with FFF stacking sequence (homogeneous piezomagnetic) has a predominant effect. This can be attributed to the fact that the pure piezomagnetic phase has higher elastic stiffness coefficients and results in increased coupling effects. Meanwhile, BBB (homogeneous piezoelectric) MEE plate shows a negligible effect. Further, the comparison of the mode shapes corresponding to different stacking arrangements of MEE plates has been depicted in Fig. 6. It can be noticed from this figure that few modes are significantly affected by the stacking sequences, whereas few remains unaffected (Pan and Heyliger 2002). This may be attributed to the various degree of coupling.

3.4 Significant combination of empirical constant

The temperature and moisture fields behave differently for the varying temperature and moisture profiles, in contrast to uniform hygrothermal loads. Hence, evaluating the significant combination of empirical constants gains importance when SMEE plate is subjected to non-uniform temperature fields. For both BFB and FBF stacking sequences with CCCC and SSSS boundary conditions, the significant combination of empirical constants are evaluated. Figs. 7(a)-7(d) illustrate the variation of fundamental natural frequency for different combinations of α^* and β^* corresponding to various SMEE plates. It can be noticed that for a constant value of α^*, the fundamental natural frequency increases with a higher value of β^*. In addition, the results tabulate in Table 7 suggests that even though a negligible discrepancies prevail, the most prominent effect is witnessed for $\alpha^*= \beta^*=2.0$. It means, a higher multiphysical frequency response can be obtained when the same values are taken for the empirical constants of temperature and moisture dependence.

3.5 Effect of temperature and moisture gradient

Meanwhile, the study is extended to analyze the effect of moisture concentration and temperature gradient. Figs. 8(a) and 8(b) depict the influence of Δm and ΔT, when ΔT and Δm are set to a constant value, respectively. From the figure it can be concluded that Δm has a minimal effect in contrast to ΔT. Therefore, the thermal field contributes more to the coupling properties than the moisture field. Figs. 9(a) -9(d) demonstrate the combined effect of Δm and ΔT considering different stacking sequences and boundary conditions. The values of the empirical constant are set to $\alpha^* = \beta^* = 1$. It can be noticed from this figure that as the value of Δm and ΔT increases, the natural frequency increases. Further, Table 8 illustrates the combined effect of Δm and ΔT for different empirical constants and skew angle. A similar conclusion with respect to skew angle, empirical constants as previously discussed can be arrived here as well.

From the previous results it is clearly witnessed that Δm and ΔT have a significant influence on the natural frequency. However, evaluating the individual effect of thermal and moisture fields and its empirical constants become important. Figs. 10(a)-10(d) show that with the increase in temperature the fundamental natural frequency increases. Analogously, Figs. 11(a)-11(d) depict the individual effect of moisture field when there is no effect of thermal field. From these figures it is revealed that, as the skew angle improves, the individual effect of both Δm and ΔT becomes higher. Also, it can be noticed that when only the moisture effect is considered, the discrepancies are more at the higher skew angle, in comparison with the individual thermal effect.

3.6 Effect of coupling

The influence of empirical constants and the individual phases on the natural frequencies of SMEE plates has been investigated. The numerical evaluation suggests that SMEE plate yields a higher natural frequency when the full coupling between elastic, electric and magnetic fields are considered. This hierarchy is followed by electro-elastic, magneto-elastic coupling. A pure elastic SMEE plate is observed to yield a minimum frequency.

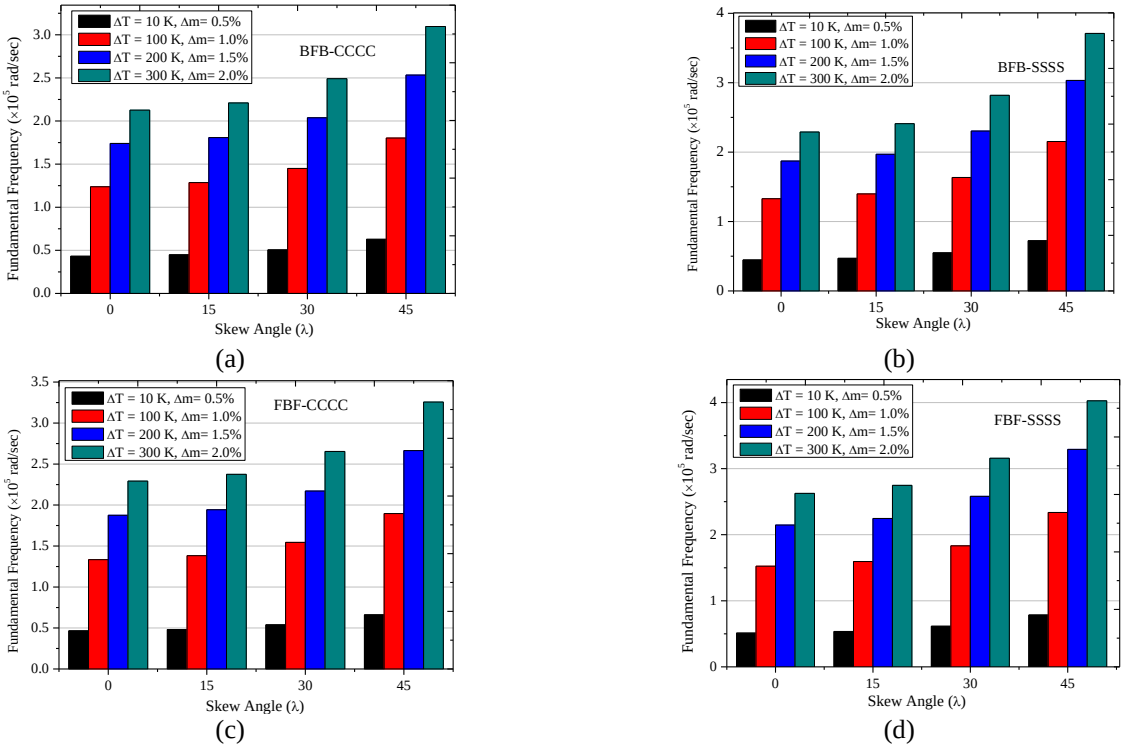

Fig. 9 Effect of different combination of ΔT and Δm on the fundamental frequency of different SMEE plates with $\alpha^* = \beta^* = 1$

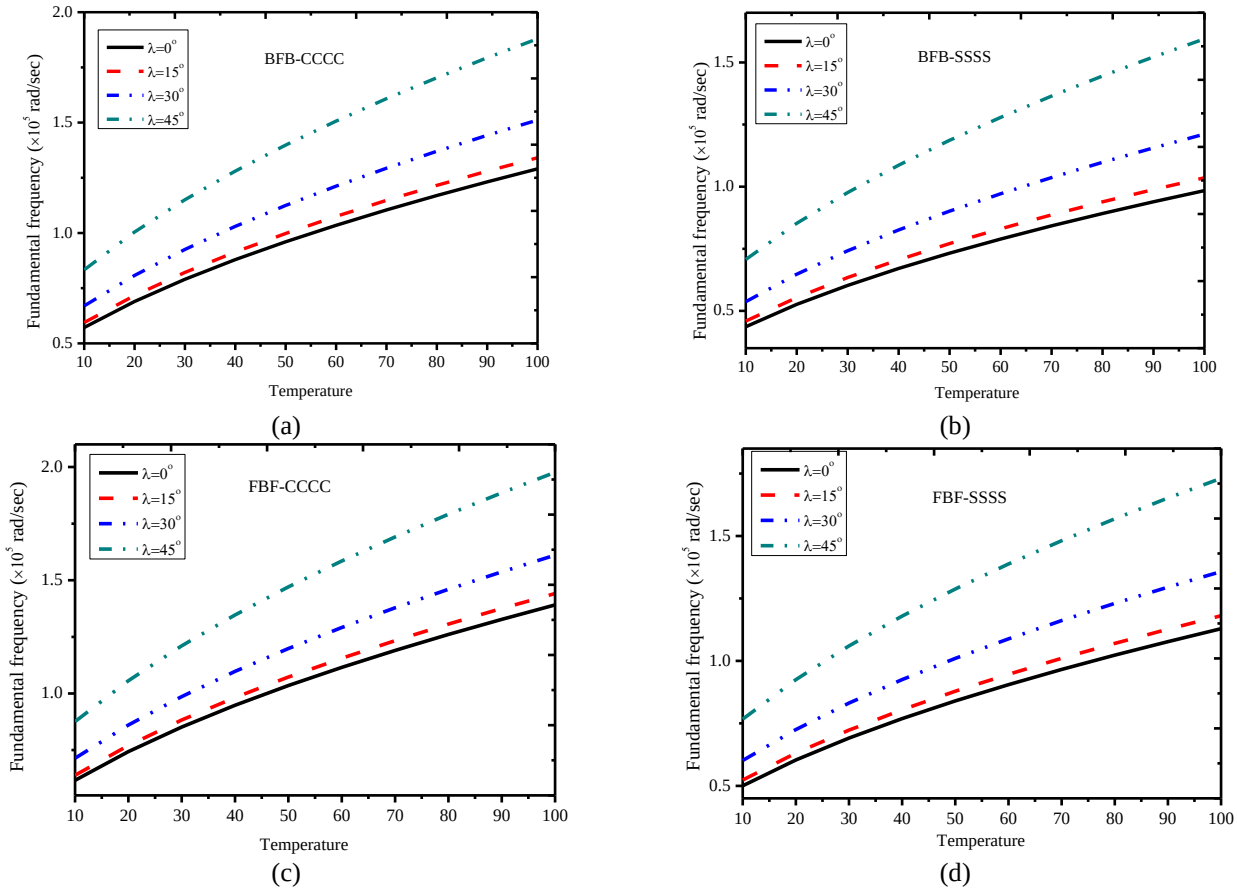

Fig. 10 Individual effect of ΔT on the fundamental frequency of different SMEE plates when Δm = 0

Table 8 Effect of different empirical constants and different combination of ΔT and Δm on the fundamental frequency of different SMEE plates

Stacking Sequence	Empirical constants	Skew Angle (λ)	Temperature and moisture rise			
			ΔT = 10 K Δm = 0.5 %	ΔT = 100 K Δm = 1 %	ΔT = 200 K Δm = 1.5 %	ΔT = 300 K Δm = 2.0 %
BFB	$\alpha^* = \beta^* = 0.5$	0^o	0.4312	1.2377	1.7397	2.1263
		15^o	0.448	1.2861	1.8077	2.2095
		30^o	0.505	1.4495	2.0375	2.4903
		45^o	0.6278	1.8023	2.5333	3.0962
	$\alpha^* = \beta^* = 1$	0^o	0.5849	1.7418	2.4542	3.0021
		15^o	0.6077	1.8099	2.5502	3.1195
		30^o	0.685	2.04	2.8743	3.516
		45^o	0.8517	2.5364	3.574	4.372
	$\alpha^* = \beta^* = 1.5$	0^o	0.7058	2.1298	3.0033	3.675
		15^o	0.7335	2.2131	3.1208	3.819
		30^o	0.8267	2.4944	3.517	4.304
		45^o	1.0278	3.1013	4.373	5.351
	$\alpha^* = \beta^* = 2.0$	0^o	0.8089	2.4572	3.466	4.242
		15^o	0.8406	2.5534	3.602	4.408
		30^o	0.9474	2.8779	4.06	4.968
		45^o	1.1779	3.578	5.048	6.177
FBF	$\alpha^* = \beta^* = 0.5$	0^o	0.4647	1.334	1.875	2.2917
		15^o	0.4815	1.3821	1.9427	2.3744
		30^o	0.5381	1.5446	2.1711	2.6536
		45^o	0.6604	1.8956	2.6644	3.2565
	$\alpha^* = \beta^* = 1$	0^o	0.6304	1.8773	2.6452	3.2357
		15^o	0.6531	1.9451	2.7406	3.3524
		30^o	0.7299	2.1738	3.0628	3.747
		45^o	0.8957	2.6677	3.759	4.598
	$\alpha^* = \beta^* = 1.5$	0^o	0.7608	2.2955	3.237	3.961
		15^o	0.7882	2.3783	3.3538	4.104
		30^o	0.8809	2.6579	3.748	4586
		45^o	1.081	3.2619	4.6	5.628
	$\alpha^* = \beta^* = 2.0$	0^o	0.8719	2.6484	3.736	4.572
		15^o	0.9033	2.744	3.871	4.737
		30^o	1.0095	3.0666	4.326	5.294
		45^o	1.2389	3.763	5.309	6.497

Table 9 Effect of coupling on the fundamental natural frequency of SMEE plate with a different stacking sequence and empirical constant (Δm = 1; ΔT = 100 K; SSSS boundary condition; $\lambda=0^o$)

Empirical Constant	Fundamental natural frequency ($\times 10^5$ rad sec^{-1})									
	BFB					FBF				
$\alpha^* = \beta^*$	MEE	EE	ME	E	Red (%)	MEE	EE	ME	E	Red (%)
0.5	0.9439	0.9123	0.9056	0.892929	5.4	1.334	1.3178	1.3022	1.2846	3.7
1	1.3284	1.2834	1.2678	1.240726	6.6	1.8773	1.8432	1.8056	1.7872	4.8
2	2.0941	1.9323	1.9031	1.888878	9.8	2.2993	2.2056	2.1567	2.1338	7.2

MEE: Magneto-electro-elastic; EE: Electro-elastic; ME: Magneto-elastic; E: Elastic; Red: Reduction % reduction = [(MEE-Elastic)/MEE] × 100

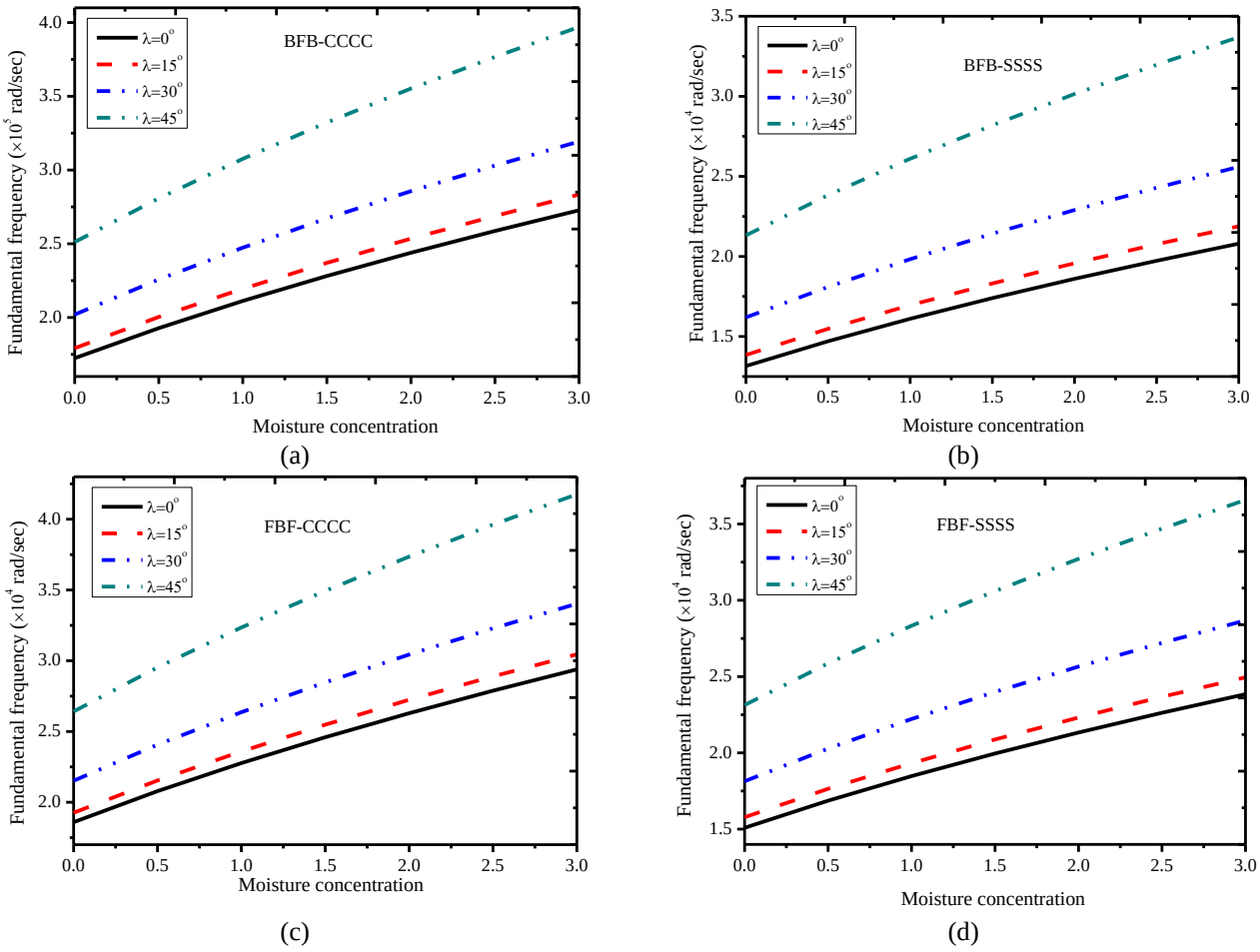

Fig. 11 Individual effect of Δm on the fundamental frequency of different SMEE plates when ΔT = 0

In addition, it is witnessed that the coupling effect are predominant for higher empirical constants as illustrated in Table 9.

3.7 Effect of boundary conditions

The effect of boundary conditions on the natural frequencies of MEE plate is evaluated.

It can be noticed from Table 6 that CCCC MEE plate has a significant influence on the characteristics of natural frequencies in contrast to the remaining boundary conditions. Further, for the temperature and moisture dependent empirical constants $\alpha^* = \beta^* = 1$, the natural frequencies variation for different combinations of ΔT and Δm for different boundary conditions are illustrated in Figs. 12(a)-12(d). In addition, the natural frequencies the MEE plate with various skew angles and empirical constants are listed in Table 10. Similar to previous evaluation, a predominant effect of higher skew angles and empirical constants can be witnessed here as well.

3.8 Effect of a/h ratio

In this section, an attempt has been made to analyse the influence of aspect ratio (*a/h*) on the free vibrations of skew MEE plate. To this end, the fundamental frequency of MEE plate with different skew angles is considered for evaluation by choosing ΔT and Δm, separately. From Figs. 13(a)-13(h) it can be witnessed that the MEE plate with lesser aspect ratio has a predominant effect. The discrepancies in the natural frequencies reduce as the aspect ratios increases. Therefore, it can be said that the aspect ratio (*a/h*) of the plate predominantly affects the stiffness properties of MEE plate. Meanwhile, it can be concluded that higher skew angle has a significant effect. Also, in contrast to the Δm a predominant influence of ΔT is noticed.

3.9 Effect of a/b ratio

The effect of the length-to-width ratio (*a/b*) on the variation of the natural frequency of MEE plates has been studied in this section. For the purpose of evaluation, BFB and FBF stacking sequences along with SSSS boundary conditions have been considered. It can be inferred from Figs. 14(a) and 14(b) that the natural frequency varies proportional to *a/b* ratio. It can be attributed to the increased stiffness of MEE plates. Meanwhile, these figures also depict that the effect of *a/h* ratio is more on the SMEE plate in contrast to rectangular MEE plates.

Table 10 Effect of boundary conditions on fundamental frequency ($\times 10^4$ rad/sec) of different SMEE plates with various empirical constants ($\Delta m = 1$; $\Delta T = 10$ K)

Stacking Sequence	Empirical constants	Skew Angle (λ)	Boundary conditions			
			CCCC	*SSSS*	*CSCS*	*CFCF*
BFB	$\alpha^* = \beta^* = 0.5$	0^o	4.312	0.1431	0.2212	0.159
		15^o	4.48	0.2073	0.2366	0.1674
		30^o	5.05	0.2705	0.2916	0.1977
		45^o	6.278	0.3987	0.4265	0.2726
	$\alpha^* = \beta^* = 1$	0^o	5.849	0.1941	0.28854	0.2157
		15^o	6.077	0.2812	0.321	0.2271
		30^o	6.85	0.3669	0.3956	0.2682
		45^o	8.517	0.5408	0.5786	0.3698
	$\alpha^* = \beta^* = 1.5$	0^o	7.058	0.2343	0.3622	0.2603
		15^o	7.335	0.3394	0.3874	0.2741
		30^o	8.267	0.4428	0.4774	0.3237
		45^o	10.27	0.6527	0.6983	0.4463
	$\alpha^* = \beta^* = 2.0$	0^o	8.809	0.2685	0.4151	0.2983
		15^o	8.406	0.389	0.444	0.3141
		30^o	9.474	0.5074	0.5471	0.3709
		45^o	11.779	0.748	0.8003	0.5115
FBF	$\alpha^* = \beta^* = 0.5$	0^o	4.647	0.1849	0.2783	0.2009
		15^o	4.815	0.2544	0.2977	0.211
		30^o	5.381	0.3371	0.3667	0.2475
		45^o	6.604	0.501	0.5365	0.339
	$\alpha^* = \beta^* = 1$	0^o	6.304	0.2508	0.3775	0.2725
		15^o	6.531	0.345	0.4038	0.2862
		30^o	7.29	0.4572	0.4974	0.3357
		45^o	8.957	0.6796	0.7277	0.4598
	$\alpha^* = \beta^* = 1.5$	0^o	7.608	0.3027	0.4556	0.3288
		15^o	7.882	0.4164	0.4873	0.3454
		30^o	8.809	0.5518	0.6003	0.4051
		45^o	10.81	0.8202	0.878	0.5549
	$\alpha^* = \beta^* = 2.0$	0^o	8.719	0.347	0.5222	0.3769
		15^o	9.033	0.4772	0.5585	0.3958
		30^o	10.095	0.6324	0.68	0.4643
		45^o	12.389	0.9432	1.007	0.636

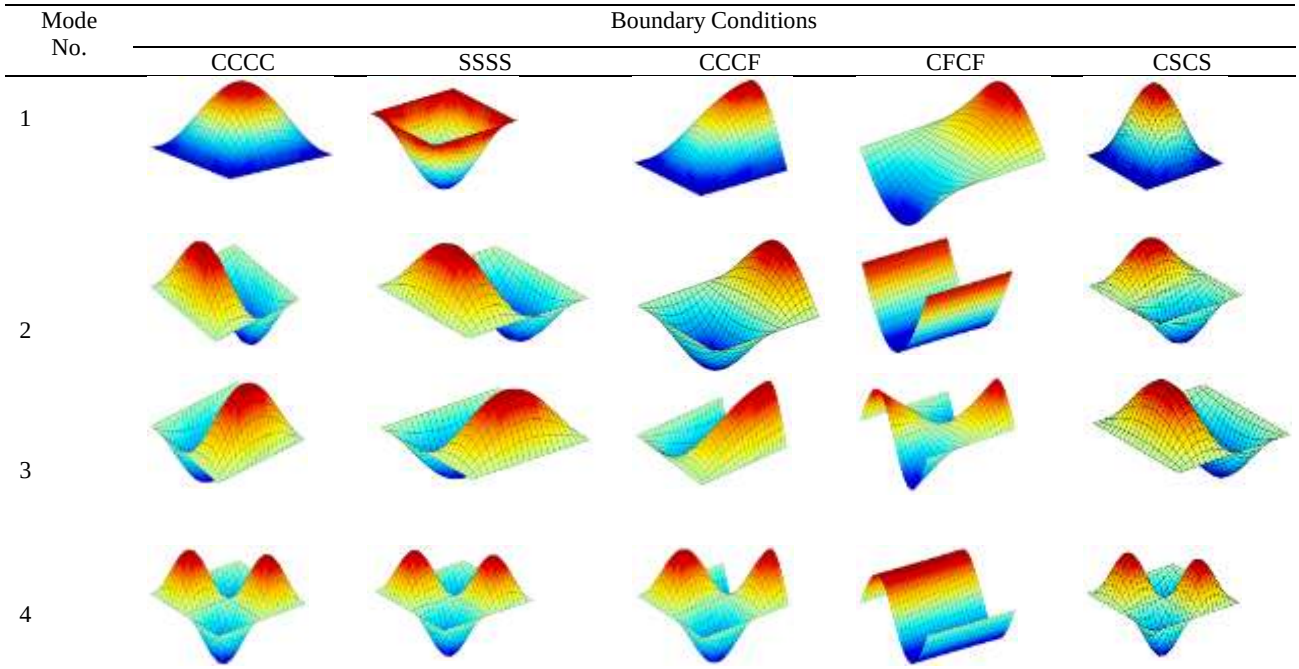

Fig. 12 Effect of boundary conditions on the mode shapes (BFB stacking sequence)

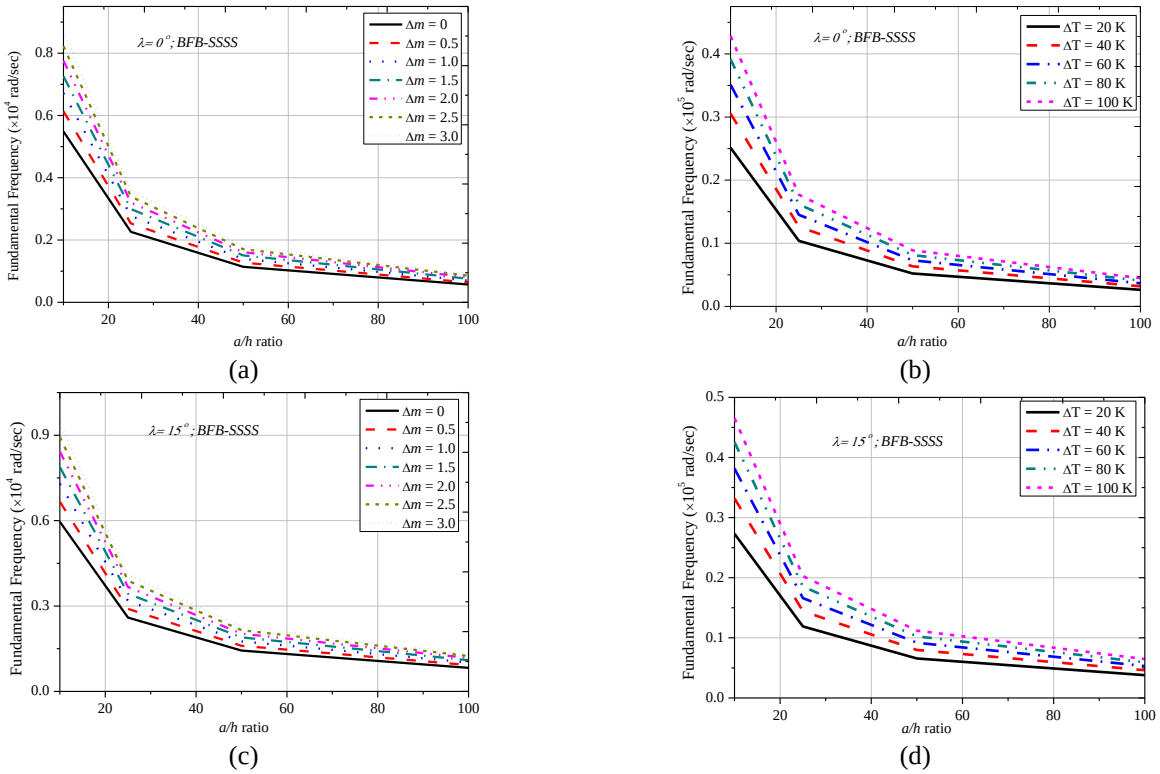

Continued-

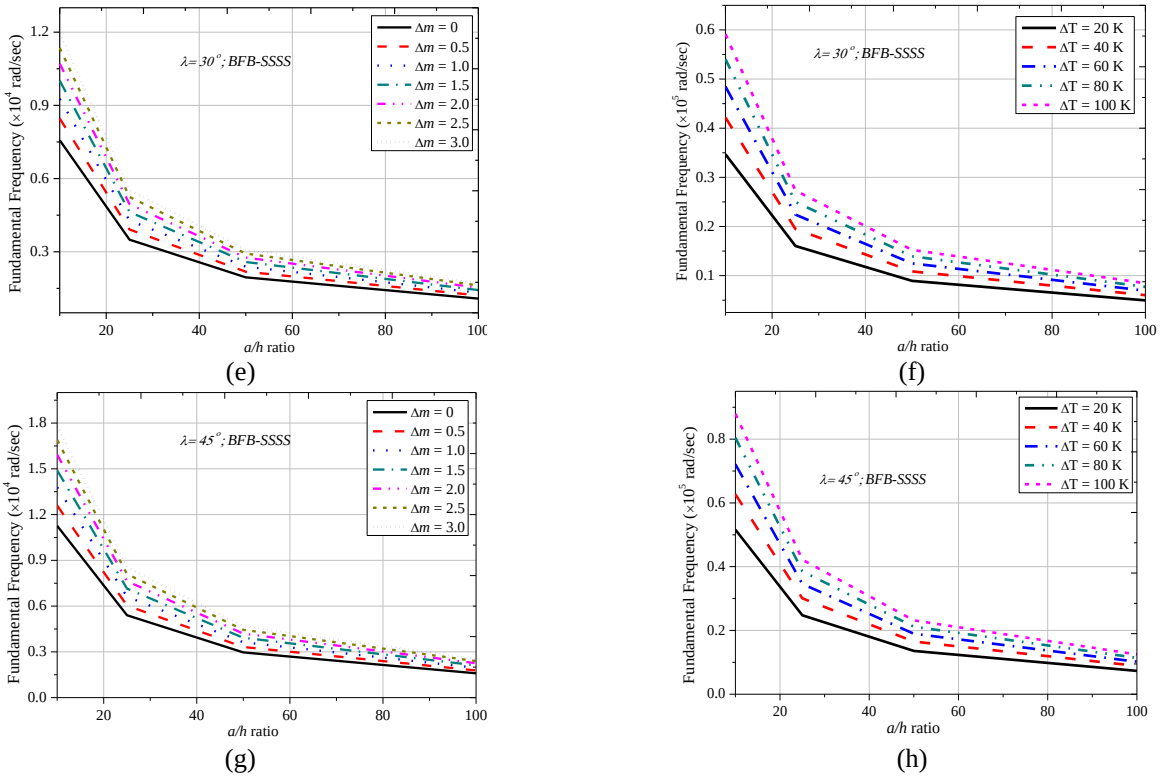

Fig. 13 Effect of aspect ratio on the different SMEE plates with different ΔT and Δm

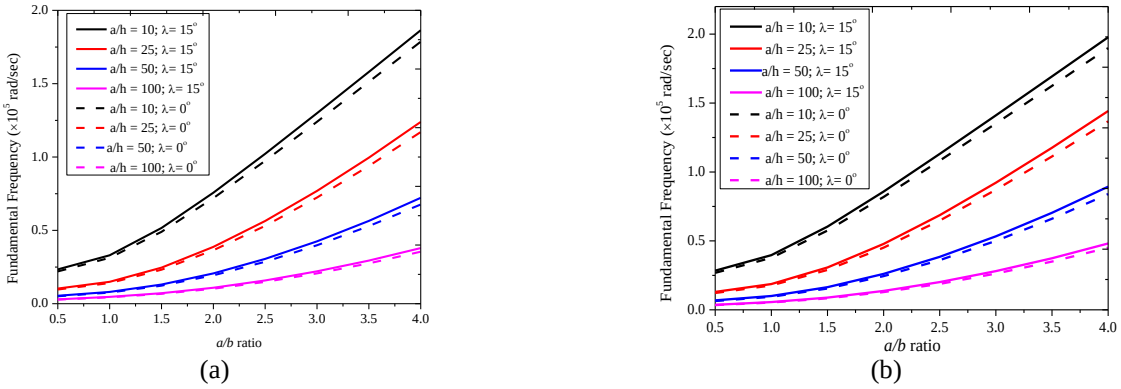

Fig. 14 Effect of length-to-width ratio on the SMEE plates with different aspect ratio and skew angle

4. Conclusions

This article deals with assessing the frequency response of skew magneto-electro-elastic plates in hygrothermal environment under the frame work of third-order shear deformation theory. To this end, a finite element formulation has been derived considering temperature and moisture dependent material properties. The equations of motion are arrived through Hamilton's principle. The numerical evaluation suggests that the frequency response is significantly affected by the skew angle and the temperature and moisture dependent empirical constants. Further, it is noticed that in comparison with the moisture concentration gradient, the natural frequency of the SMEE plate is predominantly affected by the temperature gradient. The higher value of temperature dependent empirical constant and moisture dependent empirical constant yields an increased natural frequency of MEE plate. The degree of coupling improves with the higher empirical constants. The effect of geometrical parameters such as boundary conditions, stacking sequences and aspect ratio on the free vibration characteristics has been studied. The results reveal that CCCC boundary condition has a predominant effect. Further, the MEE plates with a higher number of pure piezomagnetic phase (F) results in a greater magnitude of natural frequency and few of the higher mode shapes remain unaffected. For a given temperature and moisture concentration gradient, the natural frequencies show a significant effect for thick MEE plates (lower aspect ratio).

References

Adams, D.F. and Miller, A.K. (1977), "Hygrothermal microstresses in a unidirectional composite exhibiting inelastic material behaviour", *Compos. Mater.*, **11**, 285-299. https://doi.org/10.1177/002199837701100304.

Akbarzadeh, A.H. and Chen, Z.T. (2012), "Magnetoelectroelastic behavior of rotating cylinders resting on an elastic foundation under hygrothermal loading", *Smart Mater. Struct.*, **2**, 125013.

Akbarzadeh, A.H. and Chen, Z.T. (2013), "Hygrothermal stresses in one dimensional functionally graded piezoelectric media in constant magnetic field", *Compos. Struct.*, **97**, 317-331. https://doi.org/10.1016/j.compstruct.2012.09.058.

Akbarzadeh, A.H. and Pasini, D. (2014), "Multiphysics of multilayered and functionally graded cylinders under prescribed hygrothermomagnetoelectromechanical loading", *J. Appl. Mech.-T ASME*, **81**(4), 041018. doi: 10.1115/1.4025529.

Akbarzadeh, A. and Chen, Z. (2014), "Thermo-magneto-electro-elastic response of rotating hollow cylinders", *Mech. Adv. Mater. Struct.*, **21**(1), 67-80. https://doi.org/10.1080/15376494.2012.677108.

Alaimo, A., Milazzo, A. and Orlando, C. (2013), "A four-node MITC finite element for magneto-electro-elastic multilayered plates", *Comput.Struct.*, **129**, 120-133. https://doi.org/10.1016/j.compstruc.2013.04.014.

Annigeri, A.R, Ganesan, N. and Swarnamani, S. (2007), "Free vibration behavior of multiphase and layered magneto-electro-elastic beam", *J. Sound Vib.*, **299**(1-2), 44-63. https://doi.org/10.1016/j.jsv.2006.06.044.

Badri, T.M. and Al-Kayiem, H.H. (2013), "Analytical solution for simply supported and multilayered Magneto-Electro-Elastic Plates", *Asian J. Sci. Res.*, **6**, 236-244.

Benedetti, I. and Milazzo, A. (2017), Advanced models for smart multilayered plates based on Reissner Mixed Variational Theorem", *Compos. Part B: Eng.*, **119**, 215-229. https://doi.org/10.1016/j.compositesb.2017.03.007.

Bhangale, R.K. and Ganesan, N. (2006), "Free vibration of simply supported functionally graded and layered magneto-electro-elastic plates by finite element method", *J. Sound Vib.*, **294**(4-5), 1016-1038. https://doi.org/10.1016/j.jsv.2005.12.030.

Chen, J.Y., Heyliger, P.R. and Pan, E. (2014), "Free vibration of three-dimensional multilayered magneto-electro-elastic plates under combined clamped/free boundary conditions", *J. Sound Vib.*, **333**(17), 4017-4029. https://doi.org/10.1016/j.jsv.2014.03.035.

Chen, J., Chen, H., Pan, E. and Heyliger, P.R. (2007), "Modal analysis of magneto-electro-elastic plates using the state-vector approach", *J. Sound Vib.*, **304**(3-5), 722-734. https://doi.org/10.1016/j.jsv.2007.03.021.

Daga, A., Ganesan, N. and Shankar, K. (2009), "Behavior of magneto-electro-elastic sensors under transient mechanical loading", *Sensor. Actuat. A: Phys.*, **150**(1), 46-55. https://doi.org/10.1016/j.sna.2008.11.035.

Ebrahimi, F. and Shafiei, N. (2017), "Influence of initial shear stress on the vibration behavior of single-layered graphene sheets embedded in an elastic medium based on Reddy's higher-order shear deformation plate theory", *Mech. Adv. Mater. Struct.*, **24**(9), 761-772. https://doi.org/10.1080/15376494.2016.1196781.

Ebrahimi, F. and Barati, M.R. (2016), "Electromechanical buckling behavior of smart piezoelectrically actuated higher-order size-dependent graded nanoscale beams in thermal environment", *Int. J. Smart Nano Mater.*, **7**(2), 69-90. https://doi.org/10.1080/19475411.2016.1191556.

Huang, D.J,, Ding, H.J. and Chen, W.Q. (2007), "Analytical solution for functionally graded magneto-electro-elastic plane beams", *Int. J. Eng. Sci.*, **45**(2-8) , 467-485. https://doi.org/10.1016/j.ijengsci.2007.03.005.

Kondaiah, P., Shankar, K. and Ganesan, N. (2015), "Pyroeffects on magneto-electro-elastic sensor bonded on mild steel cylindrical shell", *Smart Struct. Syst.*, **16**(3), 537-554. https://doi.org/10.12989/sss.2015.16.3.537.

Kondaiah, P. and Shankar, K. (2017), "Pyroeffects on Magneto-Electro-Elastic Sensor patch subjected to thermal load", *Smart Struct. Syst.*, **19**(3), 299-307. https://doi.org/10.12989/sss.2017.19.3.299.

Kondaiah, P., Shankar, K. and Ganesan, N. (2012), "Studies on magneto-electro-elastic cantilever beam under thermal environment", *Coupled Syst. Mech.*, **1**(2), 205-217. https://doi.org/10.12989/csm.2012.1.2.205.

Kumaravel, A., Ganesan, N. and Sethuraman, R. (2007), "Steady-state analysis of a three-layered electro-magneto-elastic strip in a thermal environment", *Smart Mater. Struct.*, **16**(2)**,** 282-295.

Lage, R.G., Soares, C.M.M., Soares, C.A.M. and Reddy, J.N. (2004), "Layerwise partial mixed finite element analysis of magneto-electro-elastic plates", *Comput. Struct.*, **82**(17-19), 1293-1301. https://doi.org/10.1016/j.compstruc.2004.03.026.

Milazzo, A. (2013), "A one-dimensional model for dynamic analysis of generally layered magneto-electro-elastic beams", *J. Sound Vib.*, **332**(2), 465-483. https://doi.org/10.1016/j.jsv.2012.09.004.

Milazzo, A. (2014a), "Layer-wise and equivalent single layer models for smart multilayered plates", *Compos. Part B: Eng.*, **67**, 62-75. https://doi.org/10.1016/j.compositesb.2014.06.021.

Milazzo, A. (2014b), "Refined equivalent single layer formulations and finite elements for smart laminates free vibrations", *Compos. Part B: Eng.*, **61**, 238-253. https://doi.org/10.1016/j.compositesb.2014.01.055.

Moita, J.M.S., Soares, C.M.M. and Soares, C.A.M. (2009), "Analyses of magneto-electro-elastic plates using a higher order finite element model", *Compos. Struct.*, **91**(4), 421-426. https://doi.org/10.1016/j.compstruct.2009.04.007.

Ootao, Y. and Tanigawa, Y. (2005), "Transient analysis of multilayered magneto-electro-thermoelastic strip due to nonuniform heat supply", *Compos. Struct.*, **68**(4), 471-480. https://doi.org/10.1016/j.compstruct.2004.04.013.

Pan, E. (2001), "Exact solution for simply supported and multilayered magneto-electro-elastic plates", *J. Appl. Mech.- T. ASME*, **68**(4), 608-618. doi:10.1115/1.1380385.

Pan, E. and Heyliger, P.R. (2002), "Free vibrations of simply supported and multilayered magneto-electro-elastic plates", *J. Sound Vib.*, **252**(3), 429-442. https://doi.org/10.1006/jsvi.2001.3693.

Pan, E. and Han, F. (2005), "Exact solutions for functionally graded and layered magneto-electro-elastic plates", *Int. J. Eng. Sci.*, **43**(3-4), 321-339. https://doi.org/10.1016/j.ijengsci.2004.09.006.

Pan, E. and Waksmanski, N. (2016), "Deformation of a layered magnetoelectroelastic simply-supported plate with nonlocal effect, an analytical three-dimensional solution", *Smart Mater. Struct.*, **25**(9)**,** 095013.

Ramirez, F., Heyliger, P.R. and Pan, E. (2006a), "Free vibration response of two-dimensional magneto-electro-elastic laminated plates", *J. Sound Vib.*, **292**(3-5), 626-644. https://doi.org/10.1016/j.jsv.2005.08.004.

Ramirez, F., Heyliger, P.R. and Pan, E. (2006b), "Discrete layer solution to free vibrations of functionally graded magneto-electro-elastic plates", *Mech. Adv. Mater. Struct.*, **13**(3), 249-266. https://doi.org/10.1080/15376490600582750.

Razavi, S. and Shooshtari, A. (2015), "Nonlinear free vibration of magneto-electro-elastic rectangular plates", *Compos. Struct.*, **119**, 377-384. https://doi.org/10.1016/j.compstruct.2014.08.034.

Reddy, J.N. (1997), Mechanics of Laminated Composite Plates, CRC Press, Boca Raton, FL, USA.

Saadatfar, M. and Khafri, A.M. (2014), "Hygrothermomagnetoelectroelastic analysis of a functionally graded magnetoelectroelastic hollow sphere resting on an elastic foundation", *Smart Mater. Struct.*, **23**(3), 035004.

Saadatfar, M. and Khafri, A.M., (2015). "Electromagnetothermoelastic behavior of a rotating imperfect hybrid functionally graded hollow cylinder", *Smart Struct. Syst.*, **15**(6), 1411-1437. https://doi.org/10.12989/sss.2015.15.6.1411.

Shooshtari, A. and Razavi, S. (2016), "Large-amplitude free vibration of magneto-electro-elastic curved panels", *Sci. Iran.* **23**(6), 2606-2615.

Shooshtari, A. and Razavi, S. (2015a), "Large amplitude free vibration of symmetrically laminated magneto-electro-elastic rectangular plates on Pasternak type foundation", *Mech. Res. Commun.*, **69**, 103-113. https://doi.org/10.1016/j.mechrescom.2015.06.011.

Sladek, J., Sladek, V., Krahulec, S. and Pan, E. (2013a), "The MLPG analyses of large deflections of magnetoelectroelastic plates", *Eng. Anal. Bound. Elem.*, **37**(4), 673-682. https://doi.org/10.1016/j.enganabound.2013.02.001.

Sunar, M., Al-Garni, A.Z., Ali, M.H. and Kahraman, R. (2002), "Finite element modeling of thermopiezomagnetic smart structures", *AIAA J.*, **40**, 1845-1851. https://doi.org/10.2514/2.1862.

Vinyas, M., Piyush, J.S. and Kattimani, S.C. (2017a), "Influence of coupled fields on free vibration and static behavior of functionally graded magneto-electro-thermo-elastic plate", *J. Intel. Mat. Syst. Str.*, **29**(7), 1430-1455. https://doi.org/10.1177/1045389X17740739.

Vinyas, M. and Kattimani, S.C. (2017b), "Static studies of stepped functionally graded magneto-electro-elastic beam subjected to different thermal loads", *Compos. Struct.*, **163**, 216-237. https://doi.org/10.1016/j.compstruct.2016.12.040.

Vinyas, M. and Kattimani, S.C. (2017c), "A Finite element based assessment of static behavior of multiphase magneto-electro-elastic beams under different thermal loading", *Struct. Eng. Mech.*, **62**(5), 519-535. https://doi.org/10.12989/sem.2017.62.5.519.

Vinyas, M. and Kattimani, S.C. (2017d), "Static behavior of thermally loaded multilayered Magneto-Electro-Elastic beam", *Struct. Eng. Mech.*, **63**(4), 481-495. https://doi.org/10.12989/sem.2017.63.4.481.

Vinyas, M. and Kattimani, S.C. (2017e), "Multiphysics response of magneto-electro-elastic beams in thermo-mechanical environment", *Coupled Syst. Mech.*, **6**(3), 351-368. https://doi.org/10.12989/csm.2017.6.3.351.

Vinyas, M. and Kattimani, S.C. (2017f), "A 3D finite element static and free vibration analysis of magneto-electro-elastic beam", *Coupled Syst. Mech.*, **6(**4), 465-485. https://doi.org/10.12989/csm.2017.6.4.465.

Vinyas, M. and Kattimani, S.C. (2017g), "Static analysis of stepped functionally graded magneto-electro-elastic plates in thermal environment: A finite element study", *Compos. Struct.*, **178**, 63-85. https://doi.org/10.1016/j.compstruct.2017.06.068.

Vinyas, M. and Kattimani, S.C. (2017h), "Hygrothermal analysis of magneto-electro-elastic plate using 3D finite element analysis", *Compos. Struct.*, **180**, 617-637. https://doi.org/10.1016/j.compstruct.2017.08.015.

Vinyas, M. and Kattimani, S.C. (2018a), "Investigation of the effect of BaTiO3/CoFe2O4 particle arrangement on the static response of magneto-electro-thermo-elastic plates", *Compos. Struct.*, **185**, 51-64. https://doi.org/10.1016/j.compstruct.2017.10.073.

Vinyas, M. and Kattimani, S.C. (2018b), "Finite element evaluation of free vibration characteristics of magneto-electro-elastic rectangular plates in hygrothermal environment using higher-order shear deformation theory", *Compos. Struct.*, **202**, 1339-1352. https://doi.org/10.1016/j.compstruct.2018.06.069.

Vinyas, M, Kattimani, S.C., Loja, M.A.R. and Vishwas, M. (2018a), "Effect of BaTiO3/CoFe2O4micro-topological textures on the coupledstatic behaviour of magneto-electro-thermo-elastic beams indifferent thermal environment", *Mater. Res. Express*, **5**(12), 125702.

Vinyas, M., Kattimani, S.C. and Joladarashi, S. (2018b), "Hygrothermal coupling analysis of magneto-electroelastic beams using finite element methods", *J. Ther. Stresses*, **41**(8), 1063-1079. https://doi.org/10.1080/01495739.2018.1447856.

Vinyas, M., Nischith G., Loja, M.A.R., Ebrahimi, F. and Duc, N.D. (2019), "Numerical analysis of the vibration response of skew magneto-electro-elastic plates based on the higher-order shear deformation theory", *Compos. Struct.*, **214**, 132-142. https://doi.org/10.1016/j.compstruct.2019.02.010.

Vinyas, M. (2019a), "A higher order free vibration analysis of carbon nanotube-reinforced magneto-electro-elastic plates using finite element methods", *Compos. Part B*, **158**, 286-301.

Vinyas, M. (2019b), "Vibration control of skew magneto-electro-elastic plates using active constrained layer damping", *Compos. Struct.*, **208**, 600-617. https://doi.org/10.1016/j.compstruct.2018.10.046.

Wang, R. and Pan, E. (2011), "Three-dimensional modeling of functionally graded multiferroic composites", *Mech. Adv. Mater. Struct.*, **18**(1), 68-76. https://doi.org/10.1080/15376494.2010.519227.

Xin, L. and Hu, Z. (2015), "Free vibration of simply supported and multilayered magneto-electro-elastic plates", *Compos. Struct.*, **121**, 344-350. https://doi.org/10.1016/j.compstruct.2014.11.030.

Youssef, H.M. (2005), "Generalized thermoelasticity of an infinite body with a cylindrical cavity and variable material properties", *J. Therm. Stresses*, **28**(5), 521-532. https://doi.org/10.1080/01495730590925029.

CC

Appendix

The explicit representation of the stiffness matrices appearing in the Eq. (20) can be shown as follows

$$
\begin{aligned}
&\left[K^e_{tt}\right]=\left[K^e_{tb1}\right]+\left[K^e_{ts1}\right]\\
&\left[K^e_{tr}\right]=\left[K^e_{rtb24}\right]^T+\left[K^e_{rts13}\right]^T\\
&\left[K^e_{tr*}\right]=\left[K^e_{rtb4}\right]^T+\left[K^e_{rts3}\right]^T\\
&\left[K^e_{t\phi}\right]=\left[K^e_{tb\phi 1}\right]+\left[K^e_{ts\phi 1}\right]\\
&\left[K^e_{t\psi}\right]=\left[K^e_{tb\psi 1}\right]+\left[K^e_{t\psi s1}\right]\\
&\left[K^e_{rr}\right]=\left[K^e_{rrb5735}\right]+\left[K^e_{rrs3513}\right]\\
&\left[K^e_{rr*}\right]=\left[K^e_{rrb57}\right]+\left[K^e_{rrs35}\right]\\
&\left[K^e_{r\phi}\right]=\left[K^e_{rb\phi 24}\right]+\left[K^e_{r\phi s13}\right]\\
&\left[K^e_{r\psi}\right]=\left[K^e_{rb\psi 24}\right]+\left[K^e_{r\psi s13}\right]\\
&\left[K^e_{r*r*}\right]=\left[K^e_{rrb7}\right]+\left[K^e_{rrs5}\right]\\
&\left[K^e_{r*\phi}\right]=\left[K^e_{rb\phi 4}\right]+\left[K^e_{r\phi s3}\right]\\
&\left[K^e_{r*\psi}\right]=\left[K^e_{rb\psi 4}\right]+\left[K^e_{r\psi s3}\right]\\
&\left[K^e_{rrt}\right]=\left[K^e_{rtb24}\right]+\left[K^e_{rts13}\right]\\
&\left[K^e_{rrb5735}\right]=\left[K^e_{rrb57}\right]+\left[K^e_{rrb35}\right]\\
&\left[K^e_{rrs3513}\right]=\left[K^e_{rrs35}\right]+\left[K^e_{rrs13}\right]\\
&\left[K^e_{rrb57}\right]=\left[K^e_{rrb5}\right]+\left[K^e_{rrb7}\right]\\
&\left[K^e_{rrb35}\right]=\left[K^e_{rrb3}\right]+\left[K^e_{rrb5}\right]\\
&\left[K^e_{rrs35}\right]=\left[K^e_{rrs3}\right]+\left[K^e_{rrs5}\right]\\
&\left[K^e_{rrs13}\right]=\left[K^e_{rrs1}\right]+\left[K^e_{rrs3}\right]\\
&\left[K^e_{rb\phi 24}\right]=\left[K^e_{rb\phi 2}\right]+\left[K^e_{rb\phi 4}\right]\\
&\left[K^e_{r\phi s13}\right]=\left[K^e_{r\phi s1}\right]+\left[K^e_{r\phi s3}\right]\\
&\left[K^e_{rb\psi 24}\right]=\left[K^e_{rb\psi 2}\right]+\left[K^e_{rb\psi 4}\right]\\
&\left[K^e_{r\psi s13}\right]=\left[K^e_{r\psi s1}\right]+\left[K^e_{r\psi s3}\right]
\end{aligned}
\tag{A1}
$$

where

$$\left[K^e_{\psi\psi}\right]=\int_0^a\int_0^b\left[B_\psi\right]^T\left[D_{\psi\psi}\right]\left[B_\psi\right]dx\,dy,$$

$$\left[K^e_{\phi\phi}\right]=\int_0^a\int_0^b\left[B_\phi\right]^T\left[D_{\phi\phi}\right]\left[B_\phi\right]dx\,dy$$

$$\left[K^e_{tb1}\right]=\int_0^a\int_0^b\left[B_{tb}\right]^T\left[D_{b1}\right]\left[B_{tb}\right]dxdy$$

$$\left[K_{ts1}\right]=\int_0^a\int_0^b\left[B_{ts}\right]^T\left[D_{s1}\right]\left[B_{ts}\right]dxdy$$

$$\left[K^e_{rtb4}\right]=\int_0^a\int_0^b\left[B_{rb}\right]^T\left[D_{b4}\right]\left[B_{tb}\right]dxdy$$

$$\left[K^e_{rts3}\right]=\int_0^a\int_0^b\left[B_{rs}\right]^T\left[D_{s3}\right]\left[B_{ts}\right]dxdy$$

$$\left[K^e_{tb\phi 1}\right]=\int_0^a\int_0^b\left[B_{tb}\right]^T\left[D_{b\phi 1}\right]\left[B_\phi\right]dxdy$$

$$\left[K^e_{ts\phi 1}\right]=\int_0^a\int_0^b\left[B_{ts}\right]^T\left[D_{s\phi 1}\right]\left[B_\phi\right]dxdy$$

$$\left[K^e_{tb\psi 1}\right]=\int_0^a\int_0^b\left[B_{tb}\right]^T\left[D_{b\psi 1}\right]\left[B_\psi\right]dxdy$$

$$\left[K^e_{ts\psi 1}\right]=\int_0^a\int_0^b\left[B_{ts}\right]^T\left[D_{s\psi 1}\right]\left[B_\psi\right]dxdy$$

$$\left[K^e_{rrb7}\right]=\int_0^a\int_0^b\left[B_{rb}\right]^T\left[D_{b7}\right]\left[B_{rb}\right]dxdy$$

$$\left[K_{rrs5}\right]=\int_0^a\int_0^b\left[B_{rs}\right]^T\left[D_{s5}\right]\left[B_{rs}\right]dxdy$$

$$\left[K^e_{rb\phi 4}\right]=\int_0^a\int_0^b\left[B_{rb}\right]^T\left[D_{b\phi 4}\right]\left[B_\phi\right]dxdy$$

$$\left[K_{r\phi s3}\right]=\int_0^a\int_0^b\left[B_{rs}\right]^T\left[D_{s\phi 3}\right]\left[B_\phi\right]dxdy$$

$$\left[K^e_{rb\psi 4}\right]=\int_0^a\int_0^b\left[B_{rb}\right]^T\left[D_{b\psi 4}\right]\left[B_\psi\right]dxdy$$

$$\left[K_{r\psi s3}\right]=\int_0^a\int_0^b\left[B_{rs}\right]^T\left[D_{s\psi 3}\right]\left[B_\psi\right]dxdy$$

$$\left[K^e_{rrb5}\right]=\int_0^a\int_0^b\left[B_{rb}\right]^T\left[D_{b5}\right]\left[B_{rb}\right]\,dxdy$$

$$\left[K^e_{rrb7}\right]=\int_0^a\int_0^b\left[B_{rb}\right]^T\left[D_{b7}\right]\left[B_{rb}\right]\,dxdy$$

$$\left[K^e_{rrb3}\right]=\int_0^a\int_0^b\left[B_{rb}\right]^T\left[D_{b3}\right]\left[B_{rb}\right]\,dxdy$$

$$\left[K^e_{rrs1}\right]=\int_0^a\int_0^b\left[B_{rs}\right]^T\left[D_{s1}\right]\left[B_{rs}\right]\,dxdy$$

$$\left[K_{rrs3}\right]=\int_0^a\int_0^b\left[B_{rs}\right]^T\left[D_{s3}\right]\left[B_{rs}\right]\,dxdy$$

$$\left[K^e_{rrs5}\right]=\int_0^a\int_0^b\left[B_{rs}\right]^T\left[D_{s5}\right]\left[B_{rs}\right]\,dxdy$$

$$\left[K^e_{rb\phi 2}\right]=\int_0^a\int_0^b\left[B_{rb}\right]^T\left[D_{b\phi 2}\right]\left[B_{\phi}\right]\,dxdy$$

$$\left[K^e_{rb\phi 4}\right]=\int_0^a\int_0^b\left[B_{rb}\right]^T\left[D_{b\phi 4}\right]\left[B_{\phi}\right]\,dxdy$$

$$\left[K^e_{rb\psi 2}\right]=\int_0^a\int_0^b\left[B_{rb}\right]^T\left[D_{b\psi 2}\right]\left[B_{\psi}\right]\,dxdy$$

$$\left[K^e_{rb\psi 4}\right]=\int_0^a\int_0^b\left[B_{rb}\right]^T\left[D_{b\psi 4}\right]\left[B_{\psi}\right]\,dxdy$$

$$\left[K^e_{r\phi s1}\right]=\int_0^a\int_0^b\left[B_{rs}\right]^T\left[D_{s\phi 1}\right]\left[B_{\phi}\right]\,dxdy$$

$$\left[K^e_{r\phi s3}\right]=\int_0^a\int_0^b\left[B_{rs}\right]^T\left[D_{s\phi 3}\right]\left[B_{\phi}\right]\,dxdy$$

$$\left[K_{r\psi s1}\right]=\int_0^a\int_0^b\left[B_{rs}\right]^T\left[D_{s\psi 1}\right]\left[B_{\psi}\right]\,dxdy$$

$$\left[K_{r\psi s3}\right]=\int_0^a\int_0^b\left[B_{rs}\right]^T\left[D_{s\psi 3}\right]\left[B_{\psi}\right]\,dxdy$$

$$\left[K^e_{rts1}\right]=\int_0^a\int_0^b\left[B_{rs}\right]^T\left[D_{s1}\right]\left[B_{ts}\right]\,dxdy$$

$$\left[K^e_{rts3}\right]=\int_0^a\int_0^b\left[B_{rs}\right]^T\left[D_{s3}\right]\left[B_{ts}\right]\,dxdy$$

$$\left[K^e_{rtb2}\right]=\int_0^a\int_0^b\left[B_{rb}\right]^T\left[D_{b2}\right]\left[B_{tb}\right]\,dxdy$$

$$\left[F^e_{\Delta Trb4}\right]=\int_0^a\int_0^b\left[B_{rb}\right]^T\left[D_{th4}\right]\,dxdy$$

$$\left[F^e_{\Delta Trb2}\right]=\int_0^a\int_0^b\left[B_{rb}\right]^T\left[D_{th2}\right]\,dxdy$$

$$\left[F^e_{\Delta Trb1}\right]=\int_0^a\int_0^b\left[B_{tb}\right]^T\left[D_{th1}\right]\,dxdy$$

$$\left[F^e_{\Delta Trb24}\right]=\left[F^e_{\Delta Trb2}\right]+\left[F^e_{\Delta Trb4}\right]$$

$$\left[F^e_{\Delta mrb4}\right]=\int_0^a\int_0^b\left[B_{rb}\right]^T\left[D_{hy4}\right]\,dxdy$$

$$\left[F^e_{\Delta mrb2}\right]=\int_0^a\int_0^b\left[B_{rb}\right]^T\left[D_{hy2}\right]\,dxdy$$

$$\left[F^e_{\Delta mrb1}\right]=\int_0^a\int_0^b\left[B_{tb}\right]^T\left[D_{hy1}\right]\,dxdy$$

$$\left[F^e_{\Delta mrb24}\right]=\left[F^e_{\Delta mrb2}\right]+\left[F^e_{\Delta mrb4}\right]$$

$$\left[F^e_{\phi\_\Delta T}\right]=\int_0^a\int_0^b\left[B_{\phi}\right]^T\left[D_{\phi\_\Delta T}\right]\,dxdy$$

$$\left[F^e_{\phi\_\Delta m}\right]=\int_0^a\int_0^b\left[B_{\phi}\right]^T\left[D_{\phi\_\Delta m}\right]\,dxdy$$

$$\left[F^e_{\psi\_\Delta T}\right]=\int_0^a\int_0^b\left[B_{\psi}\right]^T\left[D_{\psi\_\Delta T}\right]\,dxdy$$

$$\left[F^e_{\psi\_\Delta m}\right]=\int_0^a\int_0^b\left[B_{\psi}\right]^T\left[D_{\psi\_\Delta m}\right]\,dxdy \qquad \text{(A2)}$$

The various rigidity matrices contributing to Eq. (A2) can be denoted as follows

$$\left[D_{b1}\right]=\sum_{n=1}^{N}\int_{h_n}^{h_{n+1}}\left[C_b\right]^n\,dz$$

$$[D_{b2}]=\sum_{n=1}^{N}\int_{h_n}^{h_{n+1}} z[C_b]^n\ dz$$

$$[D_{b3}]=\sum_{n=1}^{N}\int_{h_n}^{h_{n+1}} z^2[C_b]^n\ dz$$

$$[D_{b4}]=\sum_{n=1}^{N}\int_{h_n}^{h_{n+1}} c_1 z^3[C_b]^n\ dz$$

$$[D_{b5}]=\sum_{n=1}^{N}\int_{h_n}^{h_{n+1}} c_1 z^4[C_b]^n\ dz$$

$$[D_{b7}]=\sum_{n=1}^{N}\int_{h_n}^{h_{n+1}} {c_1}^2 z^6[C_b]^n\ dz$$

$$[D_{b\phi 1}]=\sum_{n=1}^{N}\int_{h_n}^{h_{n+1}} [e_b]^n\ dz$$

$$[D_{b\phi 2}]=\sum_{n=1}^{N}\int_{h_n}^{h_{n+1}} z[e_b]^n\ dz$$

$$[D_{b\phi 4}]=\sum_{n=1}^{N}\int_{h_n}^{h_{n+1}} c_1 z^3[e_b]^n\ dz$$

$$[D_{b\psi 1}]=\sum_{n=1}^{N}\int_{h_n}^{h_{n+1}} [q_b]^n\ dz$$

$$[D_{b\psi 2}]=\sum_{n=1}^{N}\int_{h_n}^{h_{n+1}} z[q_b]^n\ dz$$

$$[D_{b\psi 4}]=\sum_{n=1}^{N}\int_{h_n}^{h_{n+1}} c_1 z^3[q_b]^n\ dz$$

$$[D_{s1}]=\sum_{n=1}^{N}\int_{h_n}^{h_{n+1}} [C_s]^n\ dz$$

$$[D_{s3}]=\sum_{n=1}^{N}\int_{h_n}^{h_{n+1}} c_2 z^2[C_s]^n dz$$

$$[D_{s5}]=\sum_{n=1}^{N}\int_{h_n}^{h_{n+1}} {c_2}^2 z^4[C_s]^n dz$$

$$[D_{s\phi 1}]=\sum_{n=1}^{N}\int_{h_n}^{h_{n+1}} [e_s]^n\ dz$$

$$[D_{s\phi 3}]=\sum_{n=1}^{N}\int_{h_n}^{h_{n+1}} c_2 z^2[e_s]^n\ dz$$

$$[D_{s\psi 1}]=\sum_{n=1}^{N}\int_{h_n}^{h_{n+1}} [q_s]^n\ dz$$

$$[D_{s\psi 3}]=\sum_{n=1}^{N}\int_{h_n}^{h_{n+1}} c_2 z^2[q_s]^n\ dz$$

$$[D_{\phi\phi}]=\sum_{n=1}^{N}\int_{h_n}^{h_{n+1}} [\eta]^n\ dz;\ [D_{\psi\psi}]=\sum_{n=1}^{N}\int_{h_n}^{h_{n+1}} [\mu]^n\ dz$$

$$[D_{\phi\psi}]=\sum_{n=1}^{N}\int_{h_n}^{h_{n+1}} [m]^n\ dz$$

$$[D_{th4}]=\sum_{n=1}^{N}\int_{h_n}^{h_{n+1}} c_1 z^3[C_b]^n\ [\alpha]^n \Delta T\ dz$$

$$[D_{hy4}]=\sum_{n=1}^{N}\int_{h_n}^{h_{n+1}} c_1 z^3[C_b]^n\ [\beta]^n \Delta m\ dz$$

$$[D_{th2}]=\sum_{n=1}^{N}\int_{h_n}^{h_{n+1}} z[C_b]^n\ [\alpha]^n \Delta T\ dz$$

$$[D_{hy2}]=\sum_{n=1}^{N}\int_{h_n}^{h_{n+1}} z[C_b]^n\ [\beta]^n \Delta m\ dz$$

$$[D_{th1}]=\sum_{n=1}^{N}\int_{h_n}^{h_{n+1}} [C_b]^n[\alpha]^n \Delta T\ dz$$

$$[D_{hy1}]=\sum_{n=1}^{N}\int_{h_n}^{h_{n+1}} [C_b]^n\ [\beta]^n \Delta m\ dz$$

$$[D_{\phi\_\Delta T}]=\sum_{n=1}^{N}\int_{h_n}^{h_{n+1}} [p]^n \Delta T\ dz$$

$$[D_{\phi\_\Delta m}]=\sum_{n=1}^{N}\int_{h_n}^{h_{n+1}} [\chi]^n \Delta m\ dz$$

$$[D_{\psi\_\Delta T}]=\sum_{n=1}^{N}\int_{h_n}^{h_{n+1}} [\lambda]^n \Delta T\ dz$$

$$\left[D_{\psi\_\Delta m} \right] = \sum_{n=1}^{N} \int_{h_n}^{h_{n+1}} \left[\zeta \right]^n \Delta m \; dz \qquad \text{(A3)}$$